SANDIA REPORT
SAND2022-5649
Printed April 2022

Sandia National Laboratories

Hydrogen Plus Other Alternative Fuels Risk Assessment Models (HyRAM+) Version 4.1 Technical Reference Manual

Updated by: Brian D. Ehrhart and Ethan S. Hecht

Previous Contributors (chronological): Katrina M. Groth, Ethan S. Hecht, John T. Reynolds, Myra L. Blaylock, Erin E. Carrier, and Brian D. Ehrhart

Prepared by
Sandia National Laboratories
Albuquerque, New Mexico 87185
Livermore, California 94550

Issued by Sandia National Laboratories, operated for the United States Department of Energy by National Technology & Engineering Solutions of Sandia, LLC.

Available to DOE and DOE contractors from

U.S. Department of Energy
Office of Scientific and Technical Information
P.O. Box 62
Oak Ridge, TN 37831

Telephone: (865) 576-8401
Facsimile: (865) 576-5728
E-Mail: reports@osti.gov
Online ordering: http://www.osti.gov/scitech

Available to the public from

U.S. Department of Commerce
National Technical Information Service
5301 Shawnee Road
Alexandria, VA 22312

Telephone: (800) 553-6847
Facsimile: (703) 605-6900
E-Mail: orders@ntis.gov
Online order: https://classic.ntis.gov/help/order-methods

ABSTRACT

The HyRAM+ software toolkit provides a basis for conducting quantitative risk assessment and consequence modeling for hydrogen, methane, and propane systems. HyRAM+ is designed to facilitate the use of state-of-the-art models to conduct robust, repeatable assessments of safety, hazards, and risk. HyRAM+ integrates deterministic and probabilistic models for quantifying accident scenarios, predicting physical effects, characterizing hazards (thermal effects from jet fires, overpressure effects from delayed ignition), and assessing impacts on people. HyRAM+ is developed at Sandia National Laboratories to support the development and revision of national and international codes and standards, and to provide developed models in a publicly-accessible toolkit usable by all stakeholders.

This document provides a description of the methodology and models contained in HyRAM+ version 4.1. The two most significant changes for HyRAM+ version 4.1 from HyRAM+ version 4.0 are direct incorporation of unconfined overpressure into the QRA calculations and modification of the models for cryogenic liquid flow through an orifice. In QRA mode, the user no longer needs to input peak overpressure and impulse values that were calculated separately; rather, the unconfined overpressure is estimated for the given system inputs, leak size, and occupant location. The orifice flow model now solves for the maximum mass flux through the orifice at constant entropy while conserving energy, which does not require a direct speed of sound calculation. This does not affect the mass flow for all-gaseous releases; the method results in the same speed of sound for choked flow. However, this method does result in a higher (and more realistic) mass flow rate for a given leak size for liquid releases than was previously calculated.

ACKNOWLEDGMENT

This report describes HyRAM+, a revised version of the HyRAM code, which itself was built upon the previous work of many others. The authors therefore especially wish to thank Katrina Groth (now at the University of Maryland) for her leadership and contributions to the HyRAM project, as well as John Reynolds, Greg Walkup, and Erin Carrier for their contributions to HyRAM. The authors also wish to thank Ben Schroeder of Sandia, Cianan Sims of Sims Industries, and Jeremey Rifkin for their contributions to the HyRAM+ code. This work was supported by the U.S. Department of Energy (DOE) Office of Energy Efficiency (EERE) Hydrogen and Fuel Cell Technologies Office (HFTO), the DOE EERE Vehicles Technologies Office (VTO), and the U.S. Department of Transportation Pipeline and Hazardous Materials Safety Administration (PHMSA). The authors gratefully acknowledge Myra Blaylock, Chris LaFleur, Dusty Brooks, and Alice Muna at Sandia for helpful discussions and useful insights. The authors wish to thank Ben Schroeder, Dusty Brooks, Laura Hill, and Katrina Groth for their review of this document. The authors also wish to specifically thank the members of NFPA 2, the Hydrogen Safety Panel, and HySafe for engaging technical discussions and thoughtful feedback. Finally, the authors gratefully acknowledge the many productive discussions with users, other researchers, and the various stakeholders who have provided insight and feedback for this work.

CONTENTS

LIST OF FIGURES

LIST OF TABLES

ACRONYMS AND DEFINITIONS

AIR average individual risk

CFD computational fluid dynamics

DOE U.S. Department of Energy

EERE Office of Energy Efficiency and Renewable Energy

ESD event sequence diagram

FAR fatal accident rate

FTC failure to close

FTO failure to open

HFTO Hydrogen and Fuel Cell Technologies Office

HSE U.K. Health and Safety Executive

HyRAM Hydrogen Risk Assessment Models

HyRAM+ Hydrogen Plus Other Alternative Fuels Risk Assessment Models

MW molecular weight

NFPA National Fire Protection Association

PHMSA Pipeline and Hazardous Materials Safety Administration

PLL potential loss of life

PRD pressure relief device

QRA quantitative risk assessment

SI International System of Units

TNO Netherlands Organisation for Applied Scientific Research

TNT trinitrotoluene

VTO Vehicle Technologies Office

1. INTRODUCTION

1.1. About HyRAM+ and This Report

Hydrogen Plus Other Alternative Fuels Risk Assessment Models (HyRAM+) is a software toolkit that integrates data and methods relevant to assessing the safety of the delivery, storage, and use infrastructure of hydrogen and other alternative fuels (i.e., natural gas and propane). The HyRAM+ risk assessment calculation incorporates generic probabilities for component failures for both compressed gaseous and liquefied fuels, as well as probabilistic models for the effect of heat flux and overpressure on humans. HyRAM+ also incorporates experimentally validated models of various aspects of release and flame behavior. The HyRAM+ toolkit can be used to support multiple types of analysis, including code and standards development, safety basis development, and facility safety planning.

This report provides technical documentation of the algorithms, models, and data incorporated in HyRAM+ version 4.1. HyRAM+ version 4.1 is a revised version of the HyRAM+ version 4.0 software [1], and this report has a lot of similar content due to similarities between the two versions of the software. HyRAM+ was formerly known as the Hydrogen Risk Assessment Models (HyRAM) software, and this report and the HyRAM+ software builds off of the models and implementations from those earlier versions [2–5].

1.2. Design Goals and Limitations

HyRAM+ is designed to calculate multiple risk and harm/damage metrics from user-defined system configurations to provide insights for stakeholders in the safety, codes, and standards community [5–8]. HyRAM+ contains default inputs and fast-running, reduced-order models designed to facilitate comparison of different system designs and requirements. Reduced-order models use simplifying assumptions to approximate behavior much more quickly than more complex high-fidelity models. As such, the focus of HyRAM+ is on enabling systematic, defensible risk and consequence assessments for use in risk comparisons and sensitivity analyses, rather than a focus on absolute model accuracy.

Risk and safety assessment results should be used as part of a decision-making process, not as the sole basis for a decision. Safety and design decisions involve consideration of many factors and judgments; these factors include the safety assessments, the assumptions and limitations of safety assessments, the benefits of a technology, and public preferences. As such, HyRAM+ does not allow the user to specify an acceptability or tolerability criteria for risk or harm.

HyRAM+ is designed to enable defensible, repeatable calculations using documented algorithms. The algorithms, models, and data in HyRAM+ have been assembled from published, publicly available sources. The physics models contained in HyRAM+ have been validated against available experimental data [9–12]. Where model validation is lacking (e.g., for harm models), HyRAM+ often allows users to choose among different models. HyRAM+ includes default data for component leak frequencies, which are in most cases specific to the fuel. HyRAM+ also includes documented, expert-assigned probabilities for ignition. HyRAM+ is designed to allow users to replace the default parameters (e.g., leak frequency distribution parameters for every component) and assumptions with system-specific information when such information is available to the user.

1.3. Summary of HyRAM+ Outputs

The quantitative risk assessment (QRA) mode in HyRAM+ can be used to calculate risk metrics which are commonly used to evaluate fatality risk in multiple industries [5–8], as well as other incident frequency information:

- Fatal Accident Rate (FAR), the expected number of fatalities in 100 million exposed hours
- Average Individual Risk (AIR), the expected number of fatalities per exposed individual
- Potential Loss of Life (PLL), the expected number of fatalities per system-year
- Expected number of releases per system-year (unignited and ignited cases)
- Expected number of jet fires per system-year (immediate ignition cases)
- Expected number of overpressures per system-year (delayed ignition cases)

The physics mode of HyRAM+ can be used to calculate multiple physical effects associated with hydrogen, methane, and propane, including:

- Concentration for an unignited plume
- Jet flame temperature and trajectory
- Jet flame radiative heat flux
- Time histories of concentration, flammable mass, and overpressure due to accumulation and delayed ignition in an enclosure
- Overpressure from the delayed ignition of a jet/plume

1.4. Summary of Changes Made

HyRAM+ is an open source software, meaning that changes to the code can be observed directly[1]. However, a summary of major changes to the models will be included here for ease of reference.

The two most significant changes for HyRAM+ version 4.1 from version 4.0 are direct incorporation of unconfined overpressure into the QRA calculations and modification of the models for cryogenic liquid flow through an orifice. The unconfined overpressure model was

[1] More detailed changes are given in the source code changelog: `https://github.com/sandialabs/hyram/blob/master/CHANGELOG.md`

introduced as a standalone physics model in HyRAM+ version 4.0 [1], and now has been incorporated directly into the QRA calculations in this version. The user no longer needs to input peak overpressure and impulse values that were calculated seperately; rather, the unconfined overpressure is estimated for the given system inputs, leak size, and occupant location. These harm values are then used with the overpressure probits to estimate the probability of a fatality at each occupant location, similar to how the heat flux is estimated in the QRA for thermal harm. The second major change for HyRAM+ version 4.1 is the modification of the orifice flow model to solve for the maximum mass flux through the orifice at constant entropy while conserving energy, which does not require a direct speed of sound calculation. This does not affect the mass flow for all-gaseous releases; the method results in the same density and speed of sound for choked flow. However, this method does affect cryogenic liquid releases in which the calculation of the speed of sound for two-phase flows (while the liquid is partially flashed to a gas) is more uncertain. The new algorithm results in a higher (and more realistic) mass flow rate for a given leak size for liquid releases than was previously calculated.

Other changes include:

- Added an optional wind speed input to the jet flame analysis in Python; this is currently not available as an option in the graphical user interface (see Section 3.4.2)
- Added visible flame length as a numerical output to the physics mode flame analysis
- Added mass flow rate as a numerical output to the physics mode dispersion and unconfined overpressure analyses
- Added discharge coefficient as an input to the flame and QRA analyses
- Added phase as an input to the engineering toolkit temperature, pressure, and density calculation
- Changed the origin of unconfined overpressure blast wave to be the point at which the jet concentration is midway between the upper and lower flammability limits, instead of half the distance to the lower flammability limit (see Section 3.4.5)
- Fixed overpressure origin calculation, y- and z-coordinates were flipped
- Changed default overpressure probit model to TNO - Head Impact (see Section 2.6.2)
- Improved accuracy of calculation of flammable mass within a jet/plume by interpolating the endpoints near the rich and lean regions
- Removed unused facility height input in QRA
- Added a number of automatic tests for the QRA calculations in Python

This page intentionally left blank.

2. QUANTITATIVE RISK ASSESSMENT METHODOLOGY

In a QRA, multiple models are used together to provide a framework for reasoning about decision options, based on the input information used in those models. HyRAM+ includes a QRA mode, which provides calculations and models relevant to estimating the risk of systems for hydrogen and other alternative fuels. The consequences and fatality risk of jet flames and overpressures are estimated for different release sizes, each of which can be predicted to occur with different frequencies [5–8, 13]. These calculations use a subset of the models available in physics mode to estimate the release behavior (see Section 3).

2.1. Quantitative Risk Assessment Methodology Overview

Risk is characterized by a set of hazard exposure scenarios (i), the consequences (c_i) associated with each scenario, and the probability of occurrence (p_i) of these consequences. One commonly used expression for calculating risk is shown in Equation 1 [4, 13].

$$\text{Risk} = \sum_i (p_i \times c_i) \tag{1}$$

In a QRA, the consequences are expressed in terms of an observable quantity, such as number of fatalities or repair cost in a specific period of time. In HyRAM+, the number of fatalities is used as the safety metric of interest. Equation 1 shows risk as a product of probability; depending on the application, risk may be characterized using either probability or frequency.

2.2. Risk Metrics Calculations

There are multiple metrics used to express the fatality risk for a system under consideration. One such metric is the Potential Loss of Life (PLL), which expresses the expected number of fatalities per system-year. The PLL calculation is shown in Equation 2, where n is one of the possible safety-significant scenarios (described in Section 2.3), f_n is the frequency of that accident scenario n (described in Sections 2.3 and 2.4), and c_n is the expected number of fatalities for accident scenario n (described in Section 2.5) [5, 8].

$$\text{PLL} = \sum_n (f_n \times c_n) \tag{2}$$

Another risk metric related to the PLL is the Fatal Accident Rate (FAR), which is the expected number of fatalities in a group, per 100 million exposed hours. The FAR for a particular facility can be calculated using the PLL and the population of the facility [8]. The FAR is calculated using Equation 3, where N_{pop} is the average number of personnel in the facility, and dividing by 8760 converts from years to hours (24 hours per day and 365 days per year) [5, 13].

$$\text{FAR} = \frac{\text{PLL} \times 10^8}{\text{Exposed hours}} = \frac{\text{PLL} \times 10^8}{N_{pop} \times 8760} \tag{3}$$

The third metric used in HyRAM+ is the Average Individual Risk (AIR), which expresses the average number of fatalities per exposed individual. It is based on the number of hours the average occupant spends at the facility [8]. The AIR is calculated using Equation 4, where H is the annual number of hours the individual spends in the facility (e.g., 2000 hours for full-time worker) [5, 13].

$$\text{AIR} = H \times \text{FAR} \times 10^{-8} \tag{4}$$

2.3. Scenario Models

A release of a flammable fuel could lead to several different physical consequences and associated hazards. For continuous releases of a fuel, the physical consequences are unignited releases, jet fires (thermal effects), flash fires or fireballs (deflagration of accumulated gas dominated by thermal effects), and explosions (deflagration or detonation of accumulated gas dominated by overpressure effects) [5, 7, 8]. Currently, HyRAM+ calculates harm from thermal effects of jet fires (for immediate ignition) and overpressure (for delayed ignition). A release of a liquid fuel (e.g., liquid hydrogen or liquid natural gas) may also form a pool on the ground, but this is currently not considered in HyRAM+. These scenarios are modeled using an event sequence diagram (ESD) for release of a flammable fuel (see Figure 2-1).

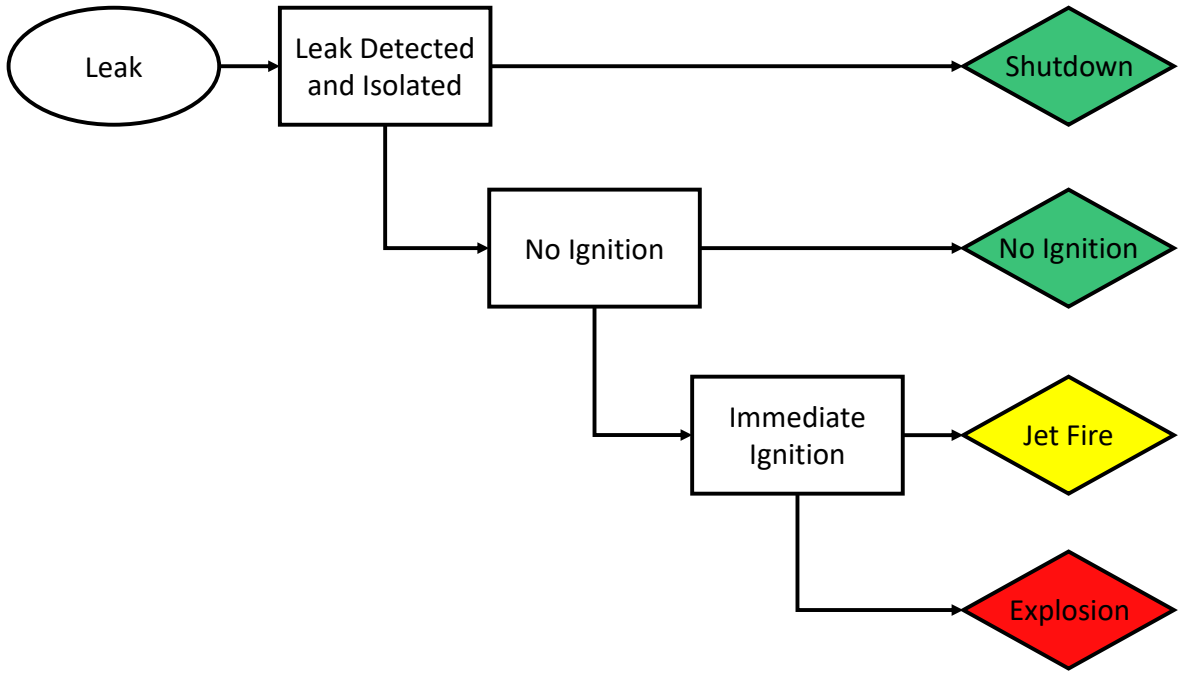

Figure 2-1 Event sequence diagram used by HyRAM+ for flammable gas releases [3].

The ESD is implemented in HyRAM+ using Equations 5–8 where f_{Release} is the annual frequency of a release (see Section 2.4), p_{Isolated} is the probability of release (leak) detection and isolation before ignition (see Section 2.3.1), $p_{\text{Immed. Ignite}}$ is the probability of immediate ignition (see Section 2.3.2), and $p_{\text{Delayed Ignite}}$ is the probability of delayed ignition (see Section 2.3.2) [3].

$$f_{\text{Isolated}} = f_{\text{Release}} \times p_{\text{Isolated}} \tag{5}$$

$$f_{\text{Unignited}} = f_{\text{Release}} \times (1 - p_{\text{Isolated}}) \times (1 - p_{\text{Immed. Ignite}} - p_{\text{Delayed Ignite}}) \tag{6}$$

$$f_{\text{Jetfire}} = f_{\text{Release}} \times (1 - p_{\text{Isolated}}) \times p_{\text{Immed. Ignite}} \tag{7}$$

$$f_{\text{Explosion}} = f_{\text{Release}} \times (1 - p_{\text{Isolated}}) \times p_{\text{Delayed Ignite}} \tag{8}$$

These equations are defined differently than is typically seen for an ESD, in which each top level event (split) in the ESD is defined with a probability and complementary probability. These equations are written in this way to utilize immediate and delayed ignition probabilities that are each defined as conditional to a leak occuring (see Section 2.3.2). Thus, there are three possible ignition outcomes, and so a top level event was added to the ESD for immediate vs. delayed ignition for ease of viewing, even if the equations are written so that the ignition probabilities in Section 2.3.2 can be used directly.

2.3.1. Default Detection and Isolation Probability

The default value for successful detection and isolation of a release (p_{Isolate}) is 0.9 [5]. This value incorporates many considerations on detection and isolation including: ventilation, sensor placement, leak location, and the ability of the sensor and isolation valve to operate successfully on demand.

Note: This value can vary significantly based on a particular system setup, and so the user/analyst needs to carefully consider the particulars of the system being assessed and decide if this default value is appropriate.

2.3.2. Default Ignition Probabilities

The default ignition probabilities are a function of release rate and are given in Table 2-1 [14]. It should be noted that both the immediate and delayed ignition probabilities are both relative to a release; the delayed ignition probability is not conditional upon the immediate ignition having not occurred. The total probability of ignition is the immediate and delayed ignition probabilities added together.

Table 2-1 Default ignition probabilities for different fuels.

(a) Hydrogen

Release Rate (kg/s)	Ignition Probability	
	Immediate	Delayed
<0.125	0.008	0.004
0.125–6.25	0.053	0.027
>6.25	0.230	0.120

(b) Methane and Propane

Release Rate (kg/s)	Ignition Probability	
	Immediate	Delayed
<1	0.007	0.003
1–50	0.047	0.023
>50	0.200	0.100

2.4. Frequency of a Release

HyRAM+ estimates the annual frequency of a release for release sizes of 0.01%, 0.1%, 1%, 10%, or 100% of pipe flow area [5–8]. These release sizes are relative to the pipe flow area (A) as shown in Equation 9, where C_d is the discharge coefficient, and d is the inner diameter of the pipe.

$$A = \frac{\pi}{4} C_d d^2 \tag{9}$$

The annual frequency of a release for each of the four smallest releases sizes ($f_{\text{Release},k}$, $k =$ 0.01%, 0.1%, 1%, and 10%) is only due to the annual frequency of random leaks ($f_{\text{Random Releases},k}$, see Section 2.4.1), as shown in Equation 10 [5, 13].

$$f_{\text{Release},k} = f_{\text{Random Releases},k} \tag{10}$$

The annual frequency of the largest release size (100%) is due to both random leaks (see Section 2.4.1) and other releases (see Section 2.4.3), as shown in Equation 11 [5].

$$f_{\text{Release, } k=100\%} = f_{\text{Random Releases, } k=100\%} + f_{\text{Other Releases}} \tag{11}$$

2.4.1. Frequency of Random Leaks

The annual frequency of random leaks is obtained for each release size using a fault tree [3]. As an example, the fault tree for random leaks for leak size 0.01% is shown in Figure 2-2. The fault trees for random leaks for all other leak sizes are analagous per leak size.

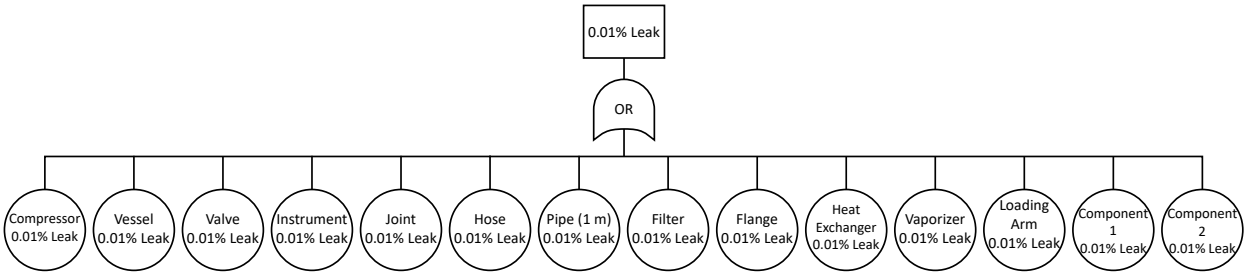

Figure 2-2 Fault tree for random leaks of size 0.01% from components.

These fault trees are implemented in HyRAM+ to combine individual component leak frequencies into an overall system leak frequency for each leak size. The annual frequency of random leaks ($f_{\text{Random Releases},k}$) is calculated using Equation 12 for each release of size k by combining the individual component leak frequencies for all the components in the system of interest, where $N_{\text{Component}_i}$ is the number of components of each type and $f_{\text{Leak}_{i,k}}$ is the leak frequency of size k for component i (see Section 2.4.2) [5]. This implementation assumes that the causes in the fault tree (leaks) are mutually exclusive.

$$f_{\text{Random Releases},k} = \sum_i N_{\text{Component}_i} \times f_{\text{Leak},i,k} \tag{12}$$

The component types are Vessels (Cylinders/Tanks), Compressors, Flanges, Hoses, Joints, Pipes[2], Valves, Filters, Instruments, Heat Exchangers, Loading Arms, Vaporizers, Extra Component #1, and Extra Component #2. Some of these components are only used for gaseous fuels (e.g., Compressors), while some are only used for liquid fuels (e.g., Vaporizers), although all are available as inputs for either gaseous or liquid fuels [1].

2.4.2. Default Component Leak Frequencies

In HyRAM+, the annual frequency of a random leak ($f_{\text{Leak},i,k}$) for component i and leak size k is assumed to be distributed as a lognormal distribution with parameters μ and σ, as noted in Equation 13 [5–8, 13].

$$f_{\text{Leak},i,k} \sim \text{Lognormal}(\mu, \sigma^2) \tag{13}$$

[2]The "Pipes" component type is per-meter of pipe; so if a system has 15 m worth of piping, then the "number" of components for that type is 15. By contrast, the "Hoses" component type is specified as per-hose, not per-length.

The geometric mean (which is equal to the median for lognormal distributions) values are used in the frequency calculations in HyRAM+ as a metric of central-tendency for the distribution[3] [3]. The geometric mean (which is equal to the median) is calculated using Equation 14.

$$\text{median} = e^{\mu} \tag{14}$$

The default values for compressed hydrogen are based on generic system leak frequencies and data from compressed hydrogen systems developed by LaChance et al. [15] and updated by both Groth et al. [13] and Glover et al. [16]. For liquid hydrogen, leak frequencies were determined using gaseous hydrogen and liquefied natural gas data as outlined by Brooks et al. [17]. For compressed methane and propane, the generic system (without the update using hydrogen data) leak frequencies described by LaChance et al. [15] are used. For liquid methane, the analysis described by Mulcahy et al. [18] was used. The μ and σ parameters were obtained from fitted distributions based on the reported distribution results from each of the original sources [1]. The default leak frequency distributions for each component are shown in Figures 2-3 and 2-4, and the default parameters and median values for the distributions are listed in Table 2-2.

There are two extra components: Extra Component #1 and Extra Component #2 which might not fall into the other component type categories [3]. The intention is that users can specify a custom leak frequency distribution for these components while still keeping the leak frequency distributions for the other components. These are meant to be set by the user.

For each component for which there is no data for a specific fuel, the mean and median leak frequencies are set to infinity, with μ and σ set to 999 to achieve this effect [1]. If a user has data for these components for a specific fuel, they can be updated. If a user does not have specific information for these components for the specific fuel of interest, leak frequency distribution parameters for another fuel or another component could be used a as a proxy. By making the default median frequency infinity, the risk metric will result in a value of infinity if one of these components is included in the system without leak frequency data, thereby alerting the user.

[3] In HyRAM+ 4.1, only the geometric mean (median) leak frequency is used in risk calculations; future versions of HyRAM+ may use additional information from the lognormal distribution in uncertainty propagation.

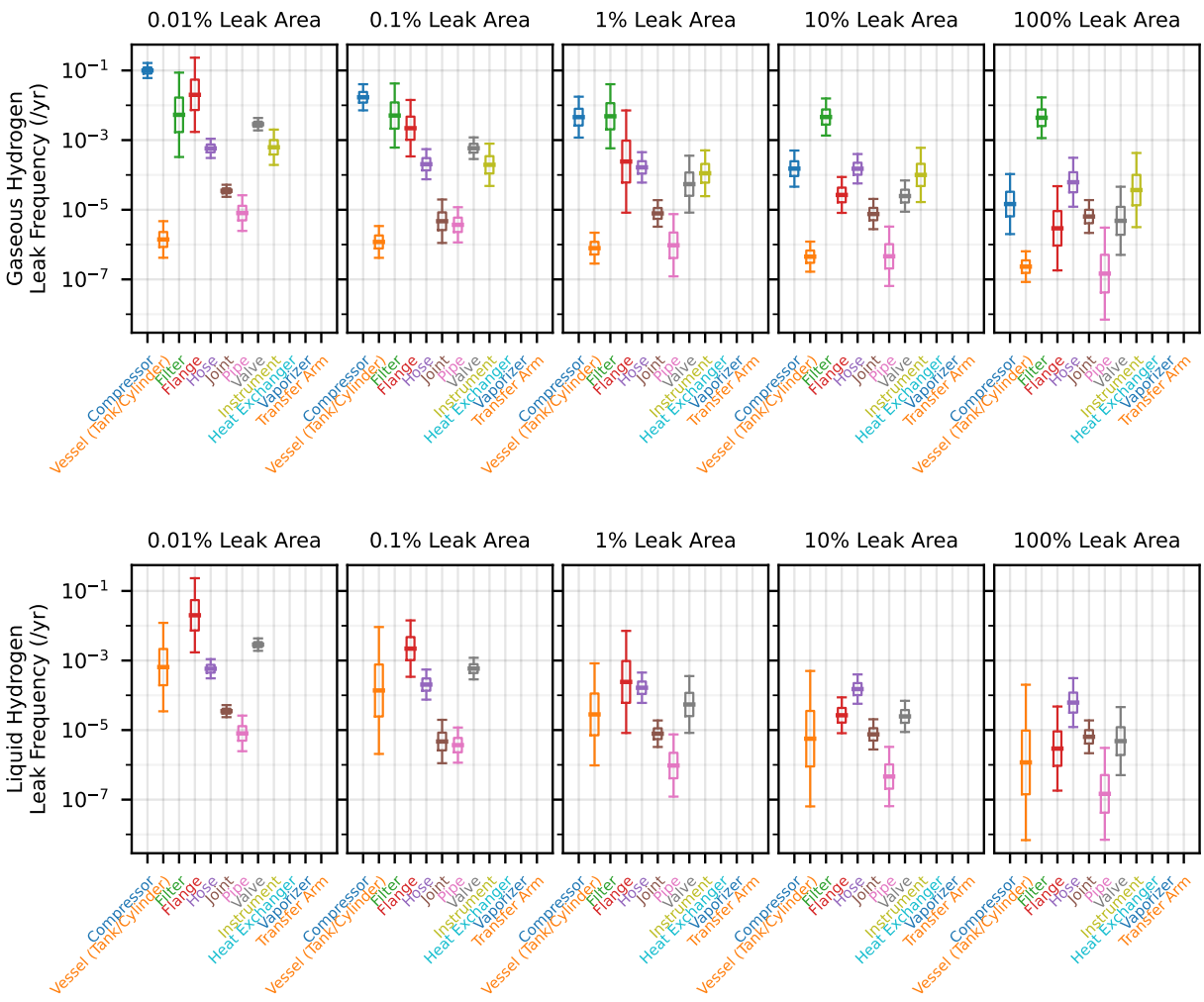

Figure 2-3 Box and whisker plots of gaseous hydrogen (top) and liquid hydrogen (bottom) leak frequencies for the different components and each leak size. The thick central line is the median leak frequency, the boxes show the 25th and 75th percentiles of the distribution and the whiskers show the 5th and 95th percentiles.

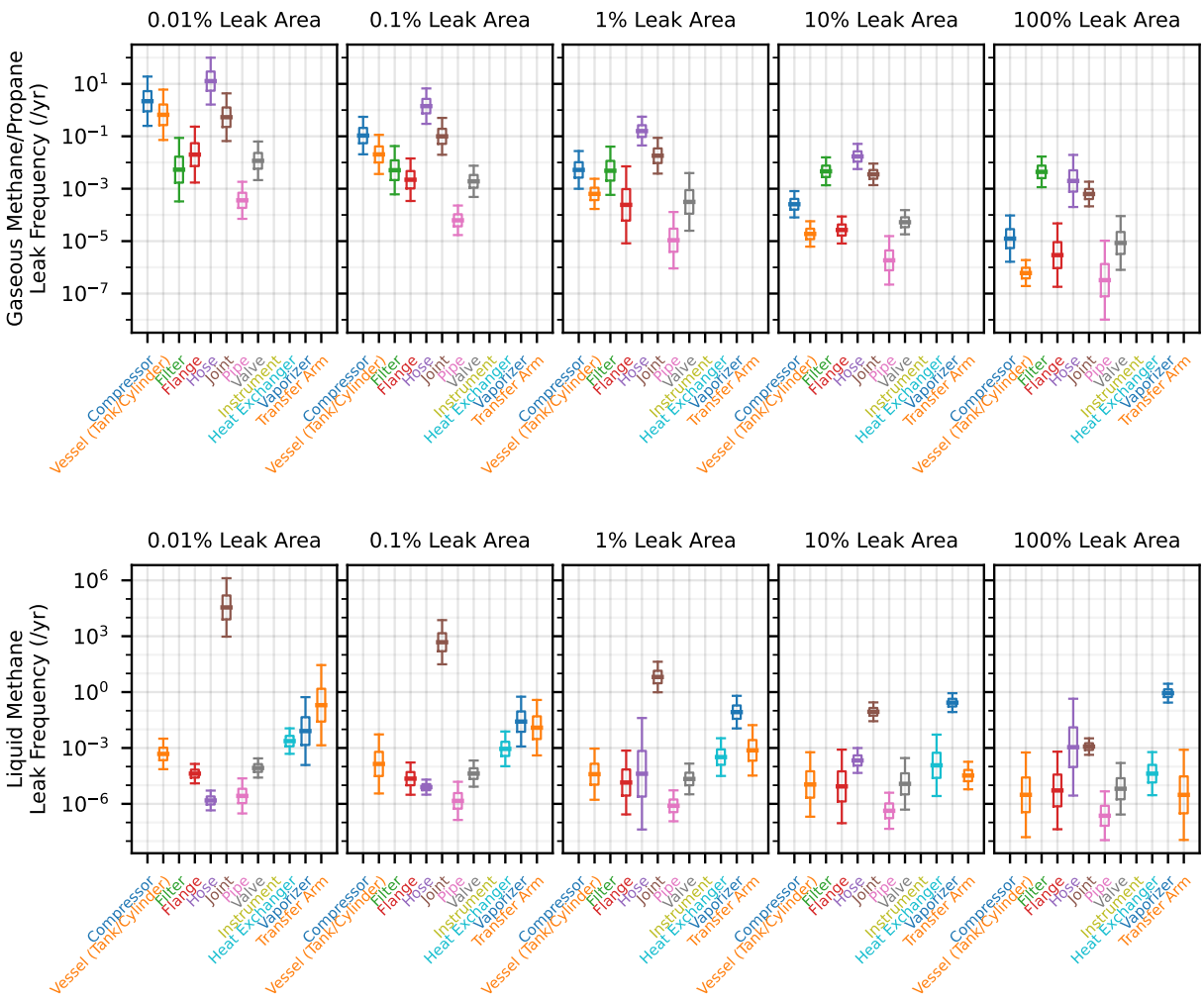

Figure 2-4 Box and whisker plots of gaseous methane and propane (top) and liquid methane (bottom) leak frequencies for the different components and each leak size. The thick central line is the median leak frequency, the boxes show the 25th and 75th percentiles of the distribution and the whiskers show the 5th and 95th percentiles.

Table 2-2 Default parameters for frequency of random leaks for individual components.

Component	Leak Size	Gaseous Hydrogen			Liquid Hydrogen			Gaseous Methane / Propane			Liquid Methane		
		μ	σ	median	μ	σ	median	μ	σ	median	μ	σ	median
Compressor	0.01%	-2.3	0.3	1.0×10^{-1}	999	999	∞	0.8	1.3	$2.2\times10^{+0}$	999	999	∞
	0.1%	-4.1	0.5	1.7×10^{-2}	999	999	∞	-2.2	1.0	1.1×10^{-1}	999	999	∞
	1%	-5.4	0.8	4.6×10^{-3}	999	999	∞	-5.3	1.0	5.2×10^{-3}	999	999	∞
	10%	-8.8	0.7	1.5×10^{-4}	999	999	∞	-8.3	0.7	2.6×10^{-4}	999	999	∞
	100%	-11.1	1.2	1.5×10^{-5}	999	999	∞	-11.3	1.2	1.2×10^{-5}	999	999	∞
Vessel (Tank/Cylinder)	0.01%	-13.5	0.7	1.4×10^{-6}	-7.3	1.8	6.5×10^{-4}	-0.4	1.3	6.6×10^{-1}	-7.6	1.1	4.8×10^{-4}
	0.1%	-13.6	0.6	1.2×10^{-6}	-8.9	2.6	1.4×10^{-4}	-3.9	1.0	2.0×10^{-2}	-8.9	2.2	1.4×10^{-4}
	1%	-14.1	0.6	7.9×10^{-7}	-10.5	2.1	2.8×10^{-5}	-7.4	0.8	6.4×10^{-4}	-10.1	1.9	3.9×10^{-5}
	10%	-14.6	0.6	4.5×10^{-7}	-12.1	2.7	5.7×10^{-6}	-10.9	0.7	1.9×10^{-5}	-11.4	2.4	1.1×10^{-5}
	100%	-15.3	0.6	2.3×10^{-7}	-13.7	3.1	1.2×10^{-6}	-14.3	0.7	6.1×10^{-7}	-12.7	3.2	3.1×10^{-6}
Filter	0.01%	-5.2	1.7	5.3×10^{-3}	999	999	∞	-5.2	1.7	5.3×10^{-3}	999	999	∞
	0.1%	-5.3	1.3	5.1×10^{-3}	999	999	∞	-5.3	1.3	5.1×10^{-3}	999	999	∞
	1%	-5.3	1.3	4.8×10^{-3}	999	999	∞	-5.3	1.3	4.8×10^{-3}	999	999	∞
	10%	-5.4	0.7	4.6×10^{-3}	999	999	∞	-5.4	0.7	4.6×10^{-3}	999	999	∞
	100%	-5.4	0.8	4.4×10^{-3}	999	999	∞	-5.4	0.8	4.4×10^{-3}	999	999	∞
Flange	0.01%	-3.9	1.5	2.0×10^{-2}	-3.9	1.5	2.0×10^{-2}	-3.9	1.5	2.0×10^{-2}	-10.1	0.7	4.2×10^{-5}
	0.1%	-6.1	1.1	2.2×10^{-3}	-6.1	1.1	2.2×10^{-3}	-6.1	1.1	2.2×10^{-3}	-10.7	1.2	2.3×10^{-5}
	1%	-8.3	2.1	2.4×10^{-4}	-8.3	2.1	2.4×10^{-4}	-8.3	2.1	2.4×10^{-4}	-11.2	2.4	1.4×10^{-5}
	10%	-10.5	0.7	2.7×10^{-5}	-10.5	0.7	2.7×10^{-5}	-10.5	0.7	2.7×10^{-5}	-11.7	2.8	8.6×10^{-6}
	100%	-12.7	1.7	2.9×10^{-6}	-12.7	1.7	2.9×10^{-6}	-12.7	1.7	2.9×10^{-6}	-12.2	2.9	5.2×10^{-6}
Hose	0.01%	-7.5	0.4	5.8×10^{-4}	-7.5	0.4	5.8×10^{-4}	2.5	1.3	$1.3\times10^{+1}$	-13.4	0.7	1.5×10^{-6}
	0.1%	-8.5	0.6	2.0×10^{-4}	-8.5	0.6	2.0×10^{-4}	0.3	0.9	$1.4\times10^{+0}$	-11.7	0.6	7.9×10^{-6}
	1%	-8.7	0.6	1.6×10^{-4}	-8.7	0.6	1.6×10^{-4}	-1.8	0.8	1.6×10^{-1}	-10.1	4.2	4.1×10^{-5}
	10%	-8.8	0.6	1.5×10^{-4}	-8.8	0.6	1.5×10^{-4}	-4.1	0.7	1.7×10^{-2}	-8.5	0.9	2.1×10^{-4}
	100%	-9.7	1.0	6.2×10^{-5}	-9.7	1.0	6.2×10^{-5}	-6.2	1.4	2.0×10^{-3}	-6.8	3.6	1.1×10^{-3}
Joint	0.01%	-10.3	0.2	3.5×10^{-5}	-10.3	0.2	3.5×10^{-5}	-0.6	1.3	5.3×10^{-1}	10.5	2.2	$3.5\times10^{+4}$
	0.1%	-12.3	0.9	4.7×10^{-6}	-12.3	0.9	4.7×10^{-6}	-2.3	1.0	1.0×10^{-1}	6.2	1.7	$4.8\times10^{+2}$
	1%	-11.8	0.5	7.9×10^{-6}	-11.8	0.5	7.9×10^{-6}	-4.0	1.0	1.8×10^{-2}	1.9	1.1	$6.5\times10^{+0}$
	10%	-11.8	0.6	7.5×10^{-6}	-11.8	0.6	7.5×10^{-6}	-5.6	0.6	3.5×10^{-3}	-2.4	0.7	8.8×10^{-2}
	100%	-12.0	0.7	6.4×10^{-6}	-12.0	0.7	6.4×10^{-6}	-7.4	0.7	6.3×10^{-4}	-6.7	0.6	1.2×10^{-3}
Pipe	0.01%	-11.7	0.7	8.0×10^{-6}	-11.7	0.7	8.0×10^{-6}	-7.9	1.0	3.6×10^{-4}	-12.8	1.3	2.7×10^{-6}
	0.1%	-12.5	0.7	3.7×10^{-6}	-12.5	0.7	3.7×10^{-6}	-9.7	0.8	6.2×10^{-5}	-13.4	1.4	1.4×10^{-6}
	1%	-13.9	1.3	9.6×10^{-7}	-13.9	1.3	9.6×10^{-7}	-11.4	1.5	1.1×10^{-5}	-14.1	1.2	7.9×10^{-7}
	10%	-14.6	1.2	4.6×10^{-7}	-14.6	1.2	4.6×10^{-7}	-13.2	1.3	1.9×10^{-6}	-14.7	1.4	4.2×10^{-7}
	100%	-15.7	1.8	1.5×10^{-7}	-15.7	1.8	1.5×10^{-7}	-14.9	2.1	3.2×10^{-7}	-15.3	1.8	2.3×10^{-7}
Valve	0.01%	-5.9	0.2	2.9×10^{-3}	-5.9	0.2	2.9×10^{-3}	-4.5	1.0	1.2×10^{-2}	-9.4	0.7	8.4×10^{-5}
	0.1%	-7.4	0.4	5.9×10^{-4}	-7.4	0.4	5.9×10^{-4}	-6.3	0.8	1.9×10^{-3}	-10.1	1.0	4.2×10^{-5}
	1%	-9.8	1.1	5.4×10^{-5}	-9.8	1.1	5.4×10^{-5}	-8.1	1.5	3.1×10^{-4}	-10.7	1.2	2.2×10^{-5}
	10%	-10.6	0.6	2.5×10^{-5}	-10.6	0.6	2.5×10^{-5}	-9.9	0.6	5.3×10^{-5}	-11.3	1.9	1.2×10^{-5}
	100%	-12.2	1.4	4.8×10^{-6}	-12.2	1.4	4.8×10^{-6}	-11.7	1.4	8.5×10^{-6}	-11.9	1.9	6.5×10^{-6}
Instrument	0.01%	-7.4	0.7	6.2×10^{-4}	999	999	∞	999	999	∞	999	999	∞
	0.1%	-8.5	0.8	2.0×10^{-4}	999	999	∞	999	999	∞	999	999	∞
	1%	-9.1	0.9	1.1×10^{-4}	999	999	∞	999	999	∞	999	999	∞
	10%	-9.2	1.1	1.0×10^{-4}	999	999	∞	999	999	∞	999	999	∞
	100%	-10.2	1.5	3.7×10^{-5}	999	999	∞	999	999	∞	999	999	∞
Heat Exchanger	0.01%	999	999	∞	999	999	∞	999	999	∞	-6.1	1.0	2.3×10^{-3}
	0.1%	999	999	∞	999	999	∞	999	999	∞	-7.0	1.3	8.9×10^{-4}
	1%	999	999	∞	999	999	∞	999	999	∞	-8.0	1.4	3.2×10^{-4}
	10%	999	999	∞	999	999	∞	999	999	∞	-9.1	2.3	1.2×10^{-4}
	100%	999	999	∞	999	999	∞	999	999	∞	-10.1	1.6	4.2×10^{-5}
Vaporizer	0.01%	999	999	∞	999	999	∞	999	999	∞	-4.8	2.5	8.1×10^{-3}
	0.1%	999	999	∞	999	999	∞	999	999	∞	-3.6	1.9	2.6×10^{-2}
	1%	999	999	∞	999	999	∞	999	999	∞	-2.5	1.2	8.4×10^{-2}
	10%	999	999	∞	999	999	∞	999	999	∞	-1.3	0.7	2.7×10^{-1}
	100%	999	999	∞	999	999	∞	999	999	∞	-0.1	0.7	8.8×10^{-1}
Transfer Arm	0.01%	999	999	∞	999	999	∞	999	999	∞	-1.6	3.0	2.0×10^{-1}
	0.1%	999	999	∞	999	999	∞	999	999	∞	-4.4	2.1	1.2×10^{-2}
	1%	999	999	∞	999	999	∞	999	999	∞	-7.2	1.9	7.5×10^{-4}
	10%	999	999	∞	999	999	∞	999	999	∞	-10.3	1.0	3.3×10^{-5}
	100%	999	999	∞	999	999	∞	999	999	∞	-12.7	3.4	3.0×10^{-6}

2.4.3. Frequency of Dispenser Releases

The annual frequency of other releases ($f_{\text{Other Releases}}$) deals with failures that can happen at a dispenser, rather than random leaks from individual components [3, 13]. The probability of an accident can be high for several reasons: fueling typically involves direct human interaction to operate the fueling dispenser, temporary connections rather than hard-plumbed lines, and inadvertently broken connections because the vehicle is not a permanent part of the system. On the other hand, releases from fueling can only occur when fueling occurs, and so different systems that involve different numbers of fueling events can be impacted by these releases to varying degrees. It is assumed that a dispenser failure would result in a large release of fuel, and so this frequency is only used in the largest (100%) leak size.

The annual frequency of other releases ($f_{\text{Other Releases}}$) is calculated using Equation 15, in which $f_{\text{Fueling Demands}}$ is the annual frequency of fueling demands (i.e., the number of times a dispenser is used to refuel a vehicle in a year) and $p_{\text{Dispenser Releases}}$ is the probability of a release from a dispenser during fueling [3]. This implementation assumes that the causes in the fault tree are mutually exclusive.

$$f_{\text{Other Releases}} = f_{\text{Fueling Demands}} \times p_{\text{Dispenser Releases}} \tag{15}$$

The annual frequency of fueling demands ($f_{\text{Fueling Demands}}$) is given by Equation 16, where N_{Vehicles} is the number of vehicles at the facility, $N_{\text{Fuelings per Day}}$ is the average number of times each vehicle is fueled per day, and $N_{\text{Operating Days per Year}}$ is the number of operating days in a year [3].

$$f_{\text{Fueling Demands}} = N_{\text{Vehicles}} \times N_{\text{Fuelings per Day}} \times N_{\text{Operating Days per Year}} \tag{16}$$

Dispenser failures are categorized in HyRAM+ as Accidents (in which the vehicle tank overpressurizes or a drive-off occurs) or Shutdown Failures (in which the system fails to shut down after a release from the nozzle) [3]. The probability for these types of releases are estimated using a fault tree as shown in Figure 2-5.

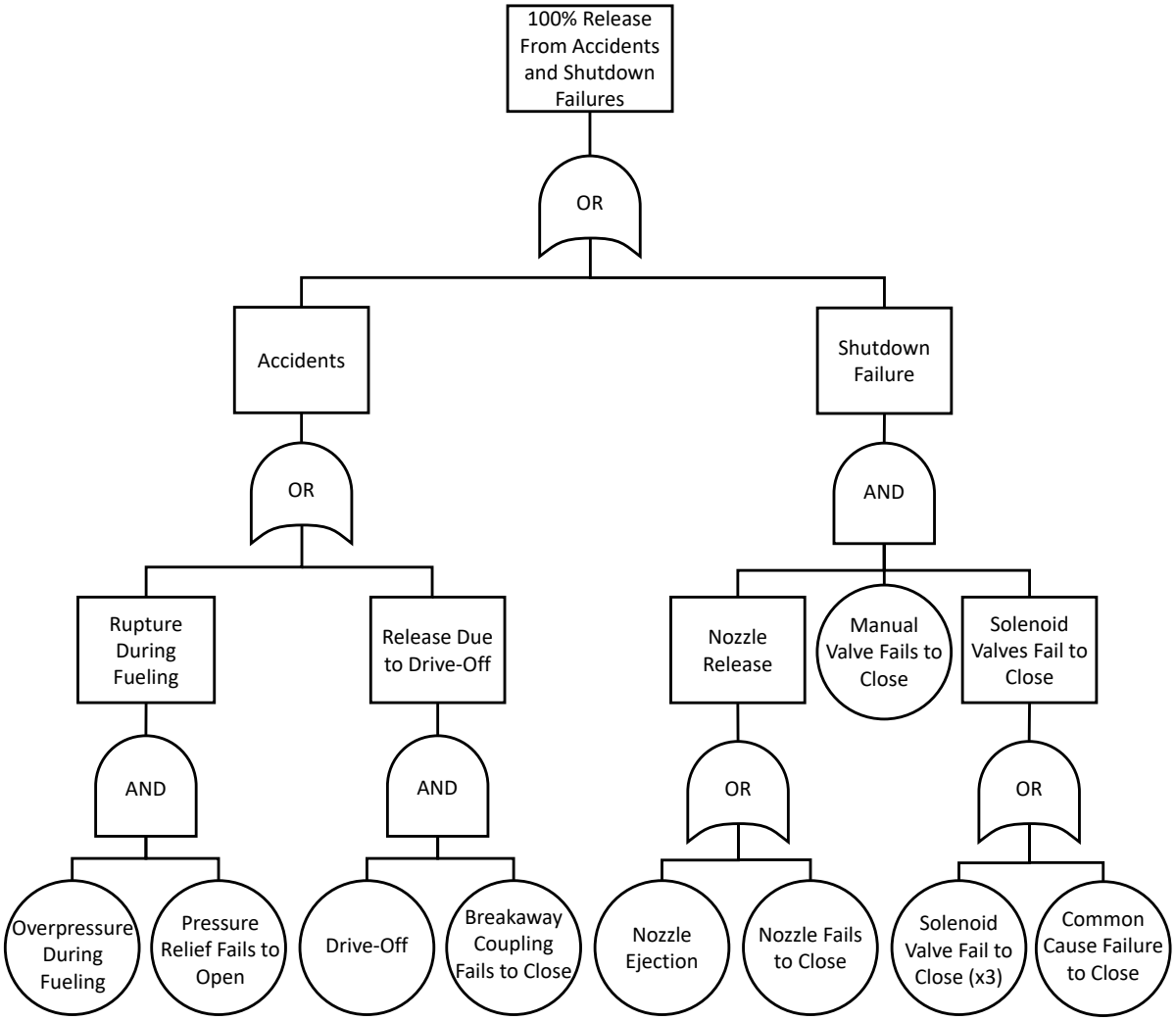

Figure 2-5 Fault tree for Other Releases from a dispenser [3].

The probability of a release from a dispenser during fueling ($p_{\text{Dispenser Releases}}$) is given by Equation 17, where $p_{\text{Accidents}}$ is the probability of an accident during fueling and $p_{\text{Shutdown Failure}}$ is the probability of a shutdown failure during fueling [3].

$$p_{\text{Dispenser Releases}} = p_{\text{Accidents}} + p_{\text{Shutdown Failure}} \tag{17}$$

The probability of an accident during fueling ($p_{\text{Accidents}}$) is given by Equation 18, where $p_{\text{Rupture During Fueling}}$ is the probability of a rupture that occurs during fueling and $p_{\text{Release Due to Drive}-\text{Off}}$ is the probability of a release occuring due to a vehicle drive-off [3].

$$p_{\text{Accidents}} = p_{\text{Rupture During Fueling}} + p_{\text{Release Due to Drive}-\text{Off}} \tag{18}$$

The probability of a rupture during fueling is given by Equation 19, in which $p_{\text{Overpressure During Fueling}}$ is the probability of an overpressure occuring during fueling (e.g., the dispenser over-fills the vehicle tank) and $p_{\text{PRD FTO}}$ is the probability of the dispenser pressure relief device failing to open on demand [3].

$$p_{\text{Rupture During Fueling}} = p_{\text{Overpressure During Fueling}} \times p_{\text{PRD FTO}} \tag{19}$$

The probabilities $p_{\text{Overpressure During Fueling}}$ and $p_{\text{PRD FTO}}$ can each be specified as a specific expected value from 0.0 to 1.0, or can be specified as a probability distribution such as Beta or Lognormal distributions. If a probability distribution is specified, the mean (or median for a lognormal distribution) value will be calculated and used in the above calculations. Default values for these probabilities are given in Section 2.4.4 [3].

The probability of a release occuring due to a vehicle drive-off ($p_{\text{Release Due to DriveOff}}$) is given by Equation 20, where p_{DriveOff} is the probability of a vehicle driving off while still attached to the dispenser during fueling and $p_{\text{Breakaway FTC}}$ is the probability of the breakaway coupling failing to close on demand [3].

$$p_{\text{Release Due to DriveOff}} = p_{\text{DriveOff}} \times p_{\text{Breakaway FTC}} \tag{20}$$

The probabilities p_{DriveOff} and $p_{\text{Breakaway FTC}}$ can each be specified as a specific expected value from 0.0 to 1.0, or can be specified as a probability distribution such as Beta or Lognormal distributions. If a probability distribution is specified, the mean (or median for a lognormal distribution) value will be calculated and used in the above calculations. Default values for these probabilities are given in Section 2.4.4.

The probability of a shutdown failure during fueling ($p_{\text{Shutdown Failure}}$) is given by Equation 21, where $p_{\text{Nozzle Release}}$ is the probability of the dispensing nozzle releasing fuel, $p_{\text{Manual Valve FTC}}$ is the probability of the manual shutoff valve failing to close on demand, and $p_{\text{Solenoid Valves FTC}}$ is the probability of the automated solenoid valves on the dispenser failing to close on demand [3].

$$p_{\text{Shutdown Failure}} = p_{\text{Nozzle Release}} \times p_{\text{Manual Valve FTC}} \times p_{\text{Solenoid Valves FTC}} \tag{21}$$

The probability of the manual shutoff valve failing to close on demand ($p_{\text{Manual Valve FTC}}$) can be specified as a specific expected value, or can be specified as a probability distribution (Beta or Lognormal) for which the mean value will be used. Default values for this probability are given in Section 2.4.4.

The probability of the dispensing nozzle releasing fuel ($p_{\text{Nozzle Release}}$) is given by Equation 22, in which $p_{\text{Nozzle Ejection}}$ is the probability of the dispenser nozzle being ejected during fueling, and $p_{\text{Nozzle FTC}}$ is the probability of the dispenser nozzle failing to close on demand [3].

$$p_{\text{Nozzle Release}} = p_{\text{Nozzle Ejection}} + p_{\text{Nozzle FTC}} \tag{22}$$

The probabilities $p_{\text{Nozzle Ejection}}$ and $p_{\text{Nozzle FTC}}$ can each be specified as a specific expected value or can be specified as a probability distribution (Beta or Lognormal) for which the mean value will be used. Default values for this probability are given in Section 2.4.4.

The probability of the automated solenoid valves on the dispenser failing to close on demand ($p_{\text{Solenoid Valves FTC}}$) is given by Equation 23, where $p_{\text{Solenoid Valve FTC}}$ is the probability of any one automated solenoid valve failing to close on demand and $p_{\text{Common Cause FTC}}$ is the probability of something causing all of the solenoid valves to fail to close on demand (e.g., loss of connection to sensors) [3].

$$p_{\text{Solenoid Valves FTC}} = [p_{\text{Solenoid Valve FTC}}]^3 + p_{\text{Common Cause FTC}} \tag{23}$$

It should be noted that this fault tree implementation assumes that there are 3 solenoid valves and that all of them need to fail in order for fuel to be released; thus, the probability for any single valve failing is cubed. These probabilities $p_{\text{Solenoid Valve FTC}}$ and $p_{\text{Common Cause FTC}}$ can each be specified as a specific expected value or can be specified as a probability distribution (Beta or Lognormal) for which the mean (or median for a lognormal distribution) value will be used. Default values for this probability are given in Section 2.4.4.

Any of the probabilities in this section can be used to estimate an annual frequency of any of the events in question. This can be done by multiplying the probability for event of interest A (p_A) by the annual number of fueling demands ($f_{\text{Fueling Demands}}$), as shown in Equation 24 [3].

$$f_A = p_A \times f_{\text{Fueling Demands}} \tag{24}$$

2.4.4. Default Dispenser Failure Probabilities

The default failure probabilities in HyRAM+ were estimated from generic data from the offshore oil, process chemical, and nuclear power industries as part of a risk assessment for indoor refueling of hydrogen-powered forklifts [13]. Table 2-3 shows the default probability distributions and parameters for various types of component failures and Table 2-4 shows the default accident occurance probability distributions and parameters for different types of accidents that are described in Section 2.4.3.

Table 2-3 Default probability distributions for component failure.

Component	Failure Mode	Distribution Type	Parameters
Nozzle	Pop-off	Beta (α, β)	$\alpha = 0.5$, $\beta = 610415.5$
Nozzle	Failure to close	Expected value	0.002
Breakaway coupling	Failure to close	Beta (α, β)	$\alpha = 0.5$, $\beta = 5031$
Pressure relief valve	Premature open	Beta (α, β)	$\alpha = 4.5$, $\beta = 310288.5$
Pressure relief valve	Failure to open	Lognormal (μ, σ)	$\mu = -11.74$, $\sigma = 0.67$
Manual valve	Failure to close (human error)	Expected value	0.001
Solenoid valve	Failure to close	Expected value	0.002
Solenoid valves	Common cause failure (3 valves, beta factor method)	Expected value	1.28×10^{-4}

Table 2-4 Default probability distributions for accident occurrence.

Accident	Distribution Type	Parameters
Drive-off	Beta (α, β)	$\alpha = 31.5$, $\beta = 610384.5$
Overpressure during fueling	Beta (α, β)	$\alpha = 3.5$, $\beta = 310289.5$

See Equation 14 for the calculation of the geometric mean (median) for a lognormal distribution. For a beta distribution with parameters α and β, the arithmetic mean is calculated using Equation 25[4].

$$\text{mean} = \frac{\alpha}{\alpha + \beta} \tag{25}$$

2.5. Consequence Models

The consequences of a leak scenario ($c_{\text{Scenario,k}}$ for $k = 0.01\%$, 0.1%, 1%, 10%, and 100%) in HyRAM+ are the estimated numbers of fatalities from each of the j occupants of the facility (see Section 2.5.1), as calculated in Equation 26.

$$c_{\text{Scenario},k} = \sum_j c_{\text{Scenario},k,j} \tag{26}$$

The consequences for each of the leak scenarios are estimated by the probability of a fatality for each of the occupants in the facility, as described in the following sub-sections.

[4]In HyRAM+ 4.1, only the mean value from the beta distribution is used in risk calculations; future versions of HyRAM+ may use additional information from the probability distribution in uncertainty propagation.

2.5.1. Facility Occupants

The harm and fatalities of interest in HyRAM+ are assumed to happen to facility occupants [3, 13]. General risk contours or risk at a specific location (such as a building or lot line) are not calculated explicitly. The risk for the entire facility is a summation of fatality risk for each of the user-specified occupant locations.

The occupant positions and number of occupants are defined by user input. For each dimension (x, y, z) for each occupant, the user may assign a position deterministically or may specify a probability distribution. Probability distributions will be randomly sampled to assign the positions using user-specified inputs to a uniform or normal distribution. The occupant positions are all defined relative to the leak point; i.e., the leak occurs at the "origin" (0, 0, 0) and extends in the positive-x direction, so the occupant positions (x, y, z) are based on that point of reference. The x and z coordinates are horizontal to the ground, while the y coordinate is height above the ground.

By default, HyRAM+ includes a set of 9 occupants that are meant to provide an example of workers within a station or facility. The locations of these default occupants are assumed to be distributed with a uniform distribution in the x-direction between 1–20 m, a constant height of 0 m (i.e., same height as the leak itself), and distributed with a uniform distribution in the z-direction between 1–12 m. These default occupants are assumed to have 2000 exposed hours per occupant per year. The number, location specifications, and exposed hours for these default occupants can be edited by the user, and additional groups with occupants with seperate number, locations, and exposed hours can be specified by the user as well.

2.5.2. Detection and Isolation Scenario Consequences

The scenario in which a leak is safely detected and isolated is assumed to result in no fatalities for all of the occupant positions [13], as shown in Equation 27.

$$c_{\text{Isolated},k,j} = 0 \tag{27}$$

2.5.3. No Ignition Scenario Consequences

The scenario in which a leak does not ignite is assumed to result in no fatalities for all of the occupant positions [13], as shown in Equation 28.

$$c_{\text{NoIgnition},k,j} = 0 \tag{28}$$

2.5.4. Jet Fire Scenario Consequences

The consequences of a jet fire on facility occupants are calculated using Equation 29, in which $p_{\text{fatal,jetfire},k,j}$ is the probability of a fatality from a jetfire for the leak size k and occupant position j.

$$c_{\text{Jetfire},k,j} = p_{\text{fatal,jetfire},k,j} \tag{29}$$

The probability of a fatality from a jetfire is described in Section 2.6, which uses physical effect modeling as described in Section 3. Specifically, the flame model described in Section 3.4.2 and multi-point radiative heat flux model described in Section 3.4.3 are used for this scenario. These models are coupled to the engineering models described in Section 3.2. The heat flux calculation is performed at each of the occupant locations, and the resulting values are then used to estimate the probability of a fatality at each of the occupant locations using the fatality probits in Section 2.6.1.

2.5.5. Overpressure Scenario Consequences

The consequences of an explosion on facility occupants are calculated using Equation 30, in which $p_{\text{fatal,explosion},k,j}$ is the probability of a fatality from an explosion for the leak size k and occupant position j.

$$c_{\text{Explosion},k,j} = p_{\text{fatal,explosion},k,j} \tag{30}$$

The probability of a fatality from an explosion is described in Section 2.6, which uses physical effect modeling as described in Section 3. The unconfined overpressure model described in Section 3.4.5 is used for this scenario. The overpressure calculation is performed at each of the occupant locations, and the resulting values are then used to estimate the probability of a fatality at each of the occupant locations using the fatality probits in Section 2.6.2.

2.6. Harm and Loss Models

Probit models are used in HyRAM+ to estimate the probability of a fatality for a given exposure [5–8, 13]. The probit model is a linear combination of predictors that model the inverse cumulative distribution function associated with the normal distribution [5, 13]. The probability of a fatality is given by Equation 31, which evaluates the standard normal cumulative distribution function (Φ)[5] at the value established by the appropriate probit model (Y, see Sections 2.6.1 and 2.6.2) [5, 13].

$$p_{\text{fatal}} = F(Y|\mu = 5, \sigma = 1) = \Phi(Y - 5) \tag{31}$$

[5]The standard normal cumulative distribution function ($\Phi(x)$) is the case in which the normal cumulative distribution function ($F(x)$) has parameters of $\mu = 0$ and $\sigma = 1$.

2.6.1. Thermal Harm

For thermal radiation, the harm level is a function of both the heat flux intensity and the duration of exposure. Harm from radiant heat fluxes is often expressed in terms of a thermal dose unit (V) which combines the heat flux intensity (I, in W/m^2) and exposure time (t, in seconds) using Equation 32 [5, 13]. The default thermal exposure time used in HyRAM+ is 60 s, but users may modify this value [5, 13].

$$V = I^{(4/3)} \times t \tag{32}$$

Table 2-5 lists the thermal probit models that are encoded in HyRAM+ [5, 13]. The probability of a fatality is evaluated using the probit value resulting from the equations in Table 2-5 with Equation 31.

Table 2-5 Probit models used to calculate fatality probability as a function of thermal dose (V).

Reference	Fatality Model	Notes
Eisenberg [19]	$Y = -38.48 + 2.56 \times \ln(V)$	Based on population data from nuclear blasts at Hiroshima and Nagasaki (ultraviolet radiation)
Tsao & Perry [20]	$Y = -36.38 + 2.56 \times \ln(V)$	Eisenberg model, modified to account for infrared radiation
TNO [21]	$Y = -37.23 + 2.56 \times \ln(V)$	Tsao and Perry model modified to account for clothing
Lees [22]	$Y = -29.02 + 1.99 \times \ln(0.5V)$	Accounts for clothing, based on porcine skin experiments using ultraviolet source to determine skin damages. Uses burn mortality information.

LaChance et al. [23] recommended using either the Eisenberg and the Tsao & Perry probit models for hydrogen-related applications. Therefore, the HyRAM+ default is the Eisenberg probit model for heat flux. This recommendation is based on the fact that hydrogen flames are less radiative than hydrocarbon flames, and so the Tsao & Perry probit model may overpredict due to the inclusion of infrared radiation. By contrast, the Tsao & Perry probit may be more relevant for hydrogencarbon fuels like methane and propane. The TNO and Lees probit accounts for clothing, which may be appropriate for some situations, though may be less conservative than the probits that do not account for clothing.

Structures and equipment can also be damaged by exposure to radiant heat flux. Some typical heat flux values and exposure times for damage to structures and components were provided by LaChance et al. [23]. However, because the exposure times required for damage is long ($>$30 min), the fatality risk due to thermal radiation from fires on structures and equipment is not generally significant since personnel are able to evacuate the building before significant structural

damage occurs [5, 13]. This is only noted because structural damage can cause physical harm (fatalities) to humans, which is the risk metric of interest within HyRAM+.

2.6.2. Overpressure Harm

There are several probit models available in HyRAM+ to predict harm and loss from blast overpressures [5, 13]. These models generally differentiate between direct and indirect effects of pressure. Significant increases in pressure can cause damage to pressure-sensitive organs such as the lungs and ears. Indirect effects include the impact from fragments and debris generated by the overpressure event and collapse of structures. Large explosions can also carry a person some distance resulting in injury from collisions with structures or from the resulting violent movement.

The probit models for the effects of overpressures that are included in HyRAM+ are provided in Table 2-6 [5]. The probability of a fatality is evaluated using the probit value resulting from the equations in Table 2-6 with Equation 31.

Table 2-6 Probit models to calculate fatality probability from exposure to overpressures, where P_s is peak overpressure (Pa) and i is the impulse of the shock wave (Pa·s).

Reference	Fatality Model
Eisenberg - Lung hemorrhage [24]	$Y = -77.1 + 6.91\ln(P_s)$
HSE - Lung hemorrhage [25, 26]	$Y = 5.13 + 1.37\ln(P_s \times 10^{-5})$
TNO - Head impact [21]	$Y = 5 - 8.49\ln[(2430/P_s) + 4.0 \times 10^8/(P_s i)]$
TNO - Structure collapse [21]	$Y = 5 - 0.22\ln[(40000/P_s)^{7.4} + (460/i)^{11.3}]$

LaChance et al. [23] recommended the use of the TNO probit models, and suggested that indirect effects from overpressure events represent the most important concern for people. The overpressures required to cause fatal lung damage are significantly higher than the values required to throw a person against obstacles or to generate missiles that can penetrate the skin. In addition, a person inside a structure would more likely be killed by the facility collapse than from lung damage [5, 13]. However, a person located outdoors would not be at risk of a structure collapse; for this reason, the HyRAM+ default is the TNO - Head Impact probit model for explosion/overpressure effects. It should be noted that some of the unconfined overpressure models in Section 3.4.5 only estimate peak overpressure, not impulse values, and so cannot be used with probit models that include an impulse term (i.e., the TNO models).

3. PHYSICS MODELS

HyRAM+ includes a physics mode, which provides models relevant to the behavior, hazards, and consequences of releases of the different fuels. Jet flames, concentration profiles for unignited jets/plumes, overpressure from the delayed ignition of a plume, and indoor accumulation with delayed ignition causing overpressure can all be investigated from the physics mode. A subset of these models is used in the QRA mode to calculate the consequences from a given release scenario, as described in Section 2.5. Several basic property calculations (e.g., the thermodynamic equation of state) are necessary to numerically simulate the release scenarios.

3.1. Properties of the Fluids

The formulations in this section describe the thermodynamic properties of unignited and ignited hydrogen, methane, and propane, which are needed to calculate different aspects of dispersion and combustion. They are described here in detail, and then referred to in subsequent sections.

3.1.1. Equation of State

Description: HyRAM+ utilizes the CoolProp library [27], called through its Python interface to perform several thermodynamic calculations. The property calculations are based on a Helmholtz energy function, and account for the real gas behavior at high pressures and at liquid (which can be cryogenic) temperatures, for liquids, gases, and two-phase mixtures. CoolProp [27] can be used to calculate the properties of hydrogen, methane, propane, air, or other fluids. For hydrogen, the relationships and energy functions are detailed in Leachman et al. [28], for methane, in Setzmann and Wagner [29], and for propane, in Lemmon et al. [30]. These thermodynamic calculations are used to calculate leak rates and are used in mass, momentum, and energy balances in regions close to the leak point. As an example, for hydrogen, the relationships between pressure[6], temperature, density, enthalpy, and entropy are plotted in Figure 3-1. In some regions of the models, the ideal gas equation of state is used, as described in other sections.

[6]HyRAM+ calculation inputs use absolute pressure, not gauge pressure

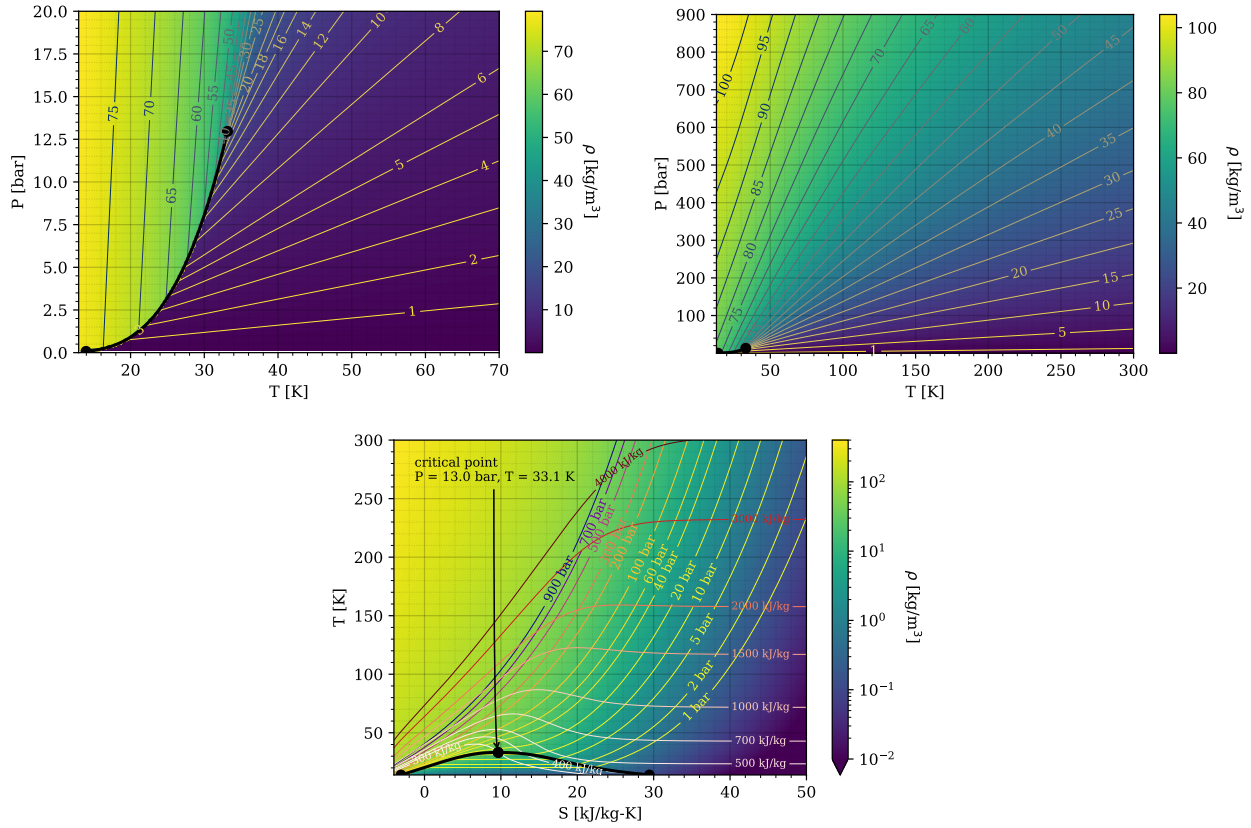

Figure 3-1 Graphical representations of state points, calculated using CoolProp [27] which uses the Leachman et al. [28] equation of state for hydrogen. Top plots show shading and iso-contours of density as a function of temperature and pressure. Bottom plot shows shading of density as a function of entropy and temperature, with iso-contours of pressure and enthalpy.

Applicability: The fundamental equation of state described by Leachman et al. [28] is valid for hydrogen at pressures up to 2000 MPa and between 14 K and 1000 K. The equation of state for methane described by Setzmann and Wagner [29] is valid from 90 K to 620 K at pressures up to 1000 MPa. The relationships described by Lemmon et al. [30] are valid for propane from 85.5 K to 650 K and for pressures up to 1000 MPa. Note that there is no check that the equation of state is being used within the stated validation limits and HyRAM+ can calculate outputs for temperatures and pressures outside the range of validity using the same equation of state.

3.1.2. Combustion

Description: HyRAM+ flame calculations are based on the work of Ekoto et al. [31] and rely on several underlying properties of burned fuel, namely the stoichiometric mixture fraction, f_s, the heat of combustion, ΔH_c, along with the temperature, molecular weight and density of combustion products for a given mixture fraction.

Assumptions: Combustion is only assumed to occur in expanded fuel at atmospheric pressure. Because combustion occurs at ambient pressure, the ideal gas equation is used to calculate the density of the product mixture (ρ) based on the molecular weight of the mixture ($MW_{mixture}$), the temperature (T), and the gas constant (R):

$$\rho = \frac{P(MW_{mixture})}{RT}. \tag{33}$$

These combustion calculations assume that there are no losses, that the mixture is thermally perfect with the local enthalpy, and the pressure of the products is the same as the pressure of the reactants.

Relationships: Stoichiometric combustion of a fuel in air (ignoring the minor species in air) can be written as

$$C_nH_{2n+2} + \frac{3n+1}{2}(O_2 + 3.76N_2) \rightarrow (n+1)H_2O_{(g)} + nCO_2 + 1.88(3n+1)N_2. \tag{34}$$

During combustion, 242 kJ is released for every mole of gaseous water produced, and 394 kJ is released for every mole of carbon dioxide produced [32]. Therefore, when $n = 0$ and hydrogen is the fuel, the heat of combustion is 242 kJ/mol_{H_2} or 120 MJ/kg_{H_2} (using the lower heating value) [33, 34]. For methane and propane, the heats of combustion are 50 MJ/kg and 46.4 MJ/kg, respectively. From Equation 34, the stoichiometric mixture fraction (f_s), which is the same as the mass fraction of fuel, can be calculated as:

$$f_s = \frac{MW_{C_nH_{2n+2}}}{MW_{C_nH_{2n+2}} + \frac{3n+1}{2}(MW_{O_2} + 3.76MW_{N_2})}. \tag{35}$$

The stoichiometric mixture fractions for hydrogen, methane, and propane are 0.02852, 0.05519, and 0.06034 respectively. If incomplete combustion occurs (a mixture fraction other than stoichiometric), there will be excess air or fuel on the right hand side of Equation 34 at the temperature of the product stream. In other words,

$$\begin{aligned} C_nH_{2n+2} + \eta\frac{3n+1}{2}(O_2 + 3.76N_2) \rightarrow & \max(0, 1-\eta)C_nH_{2n+2} \\ & + \min(1, \eta(n+1))H_2O + \min(1, \eta n)CO_2 \\ & + \max\left(0, (\eta-1)\frac{3n+1}{2}\right)O_2 + 3.76\eta\frac{3n+1}{2}N_2, \end{aligned} \tag{36}$$

where η, which specifies the moles of air, can vary from 0 to ∞. In this case, the mixture fraction is equal to

$$f = Y_{C_nH_{2n+2}} + Y_{H_2O}\frac{MW_{C_nH_{2n+2}}}{MW_{H_2O}} + Y_{CO_2}\frac{MW_{C_nH_{2n+2}}}{MW_{CO2}}, \tag{37}$$

where Y is the mass fraction of products or reactants. HyRAM+ uses CoolProp [27] to calculate the enthalpy (h) of H_2, H_2O, CO_2, O_2, and N_2 as a function of temperature and then solves for the

temperature of products assuming an isenthalpic reaction, i.e.,

$$\sum_{i=\mathrm{C_nH_{2n+2}},\mathrm{O_2},\mathrm{N_2}} Y_{i,\mathrm{reac}} h_{i,\mathrm{reac}}(T_{\mathrm{reac}}, P_{\mathrm{reac}}) = \sum_{i=\mathrm{C_nH_{2n+2}},\mathrm{O_2},\mathrm{N_2},\mathrm{CO_2},\mathrm{H_2O}} Y_{i,\mathrm{prod}} h_{i,\mathrm{prod}}(T_{\mathrm{prod}}, P_{\mathrm{prod}}) + Y_{\mathrm{H_2O,prod}} \frac{\mathrm{MW_{C_nH_{2n+2}}}}{(\mathrm{n}+1)\mathrm{MW_{H_2O}}} \Delta H_c. \quad (38)$$

The calculation of the adiabatic flame temperature (T_{ad}) and density of the products of 298 K, 101,325 Pa fuels are shown in Figure 3-2.

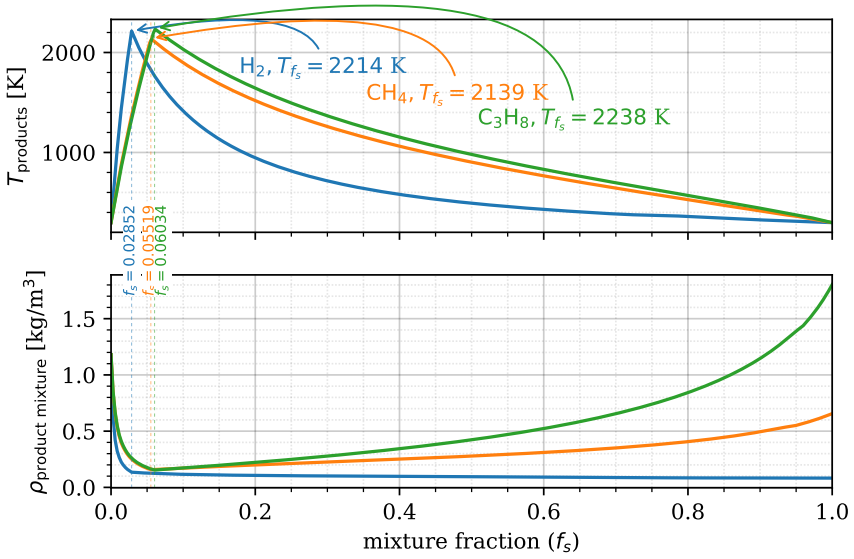

Figure 3-2 Temperature and density of products for the combustion of 298 K, 101,325 Pa fuels as a function of mixture fraction.

Applicability: These combustion calculations are applicable in atmospheric pressure regions where heat losses are negligible.

3.2. Developing Flow

Several engineering models are used in HyRAM+ to develop boundary conditions for the integral models of jets/plumes and diffusion flames. These engineering models describe the flow through an orifice, how the fluid expands to atmospheric pressure (if necessary), how the fluid warms to a level that the equation of state is valid (if necessary), and finally how the flow develops into the Gaussian profiles that serve as the boundary conditions to the models described in Sections 3.3.1 and 3.4.2.

3.2.1. Orifice Flow

HyRAM+ assumes that fluids flow isentropically through an orifice. CoolProp [27] is used to calculate the entropy (s_0) and enthalpy (h_0) of the fluid upstream of an orifice, using the specified pressure and temperature (or phase if a saturated vapor or saturated liquid is specified). CoolProp [27] is then used to calculate the enthalpy (h) and density (ρ) of a fluid at a given pressure with the same entropy as the upstream fluid (s_0). An isenthalpic expansion requires

$$\frac{v^2}{2} + h = h_0 \tag{39}$$

which can be solved for the velocity, v, and the mass flux can be calculated as

$$\dot{m}'' = \rho v. \tag{40}$$

A maximum mass flux is sought between the ambient and upstream pressures [35–37] using a bounded solver. If the maximum mass flux occurs at atmospheric pressure, the flow is unchoked, while if the maximum mass flux is at a pressure above atmospheric, the flow is choked. In the case of choked flow, the velocity through the orifice will be the speed of sound for the given throat conditions. The choked flow speed of sound for gases is the same as that calculated by CoolProp [27], but this algorithm also works for two-phase and liquid flows through the throat, for which the speed of sound is ill-defined.

Orifices in HyRAM+ are assumed to be circular, characterized by their diameter, d, and a coefficient of discharge, C_d. When the velocity and density of the fluid at the orifice is known, the mass flow rate is calculated as:

$$\dot{m} = \frac{\pi}{4} d^2 \dot{m}'' C_d = \frac{\pi}{4} d^2 \rho v C_d. \tag{41}$$

3.2.2. Notional Nozzles

Notional nozzles are used to calculate the effective diameter, velocity, and thermodynamic state after the complex shock structure of an under-expanded jet. In HyRAM+, a notional nozzle model is used if the pressure at the orifice is above atmospheric pressure. They are not necessarily a physical description of the phenomena, but a jet with the diameter, velocity and state (temperature and atmospheric pressure) of the notional nozzle would lead to the same dispersion characteristics as the underexpanded jet. There are five different notional nozzle models in HyRAM+, with each model conserving mass between flow through the real orifice and flow through the notional nozzle. This means that

$$\rho_{\text{eff}} v_{\text{eff}} A_{\text{eff}} = \rho_{\text{throat}} v_{\text{throat}} A_{\text{throat}} C_D \tag{42}$$

where ρ is the density, v is the velocity, A is the cross-sectional area, C_D is the discharge coefficient, the subscript "throat" denotes the choke point (at the orifice, see Section 3.2.1), and the subscript "eff" denotes effective (after the shock structure and the pressure has returned to atmospheric).

The default notional nozzle model in HyRAM+ is based on the work of Yüceil and Ötügen [38]. In this case, mass (Equation 42), momentum, and energy are conserved. Conservation of momentum is written as

$$\rho_{\text{eff}} v_{\text{eff}}^2 A_{\text{eff}} = \rho_{\text{throat}} v_{\text{throat}}^2 A_{\text{throat}} C_D + A_{\text{throat}} (P_{\text{throat}} - P_{\text{ambient}}) \tag{43}$$

where P is the pressure. Simultaneous solution of Equations 42 and 43 yields a solution for the velocity at the notional nozzle

$$v_{\text{eff}} = v_{\text{throat}} C_D + \frac{P_{\text{throat}} - P_{\text{ambient}}}{\rho_{\text{throat}} v_{\text{throat}} C_D} \tag{44}$$

and the effective area of the notional nozzle

$$A_{\text{eff}} = \frac{\rho_{\text{throat}} v_{\text{throat}}^2 A_{\text{throat}} C_D^2}{\rho_{\text{eff}} \left(P_{\text{throat}} - P_{\text{ambient}} + \rho_{\text{throat}} V_{\text{throat}}^2 C_D^2 \right)} \tag{45}$$

Close examination of Equation 45 shows that the area calculation requires the effective density. The density is calculated using the conservation of energy (assuming isentropic expansion), where

$$\frac{v_{\text{eff}}^2}{2} + h(\rho_{\text{eff}}, P_{\text{ambient}}) = \frac{v_{\text{throat}}^2}{2} + h_{\text{throat}} \tag{46}$$

CoolProp [27] is used to calculate the enthalpy and Equation 46 is solved to determine the effective density.

Alternative to using Equation 46, the second notional nozzle model follows the work of Birch et al. (1987) [39]. In this work, the effective density is calculated by assuming that the temperature of the notional nozzle is the same as the temperature of the stagnant gas, or

$$\rho_{\text{eff}} = \rho(T_0, P_{\text{ambient}}) \tag{47}$$

where T_0 is the temperature of the stagnant gas (storage temperature) and CoolProp [27] is used to calculate the density.

Three other notional nozzle models do not conserve momentum (Equation 43), but rather assume that the notional nozzle velocity is at the speed of sound, as follows. The third notional nozzle model follows the work of Birch et al. (1984) [40]. For this model, it is assumed that the temperature at the notional nozzle is the same as temperature of the stagnant gas, the density (see Equation 47) and velocity at the notional nozzle can be calculated

$$v_{\text{eff}} = a(T_0, P_{\text{ambient}}) \tag{48}$$

where a is the speed of sound, calculated using CoolProp [27]. The conservation of mass, Equation 42, along with Equations 47 and 48, can be used to specify the notional nozzle conditions.

Alternatively, Ewan and Moody [41] use the assumption that the temperature at the notional nozzle is the same as the temperature at the throat, or

$$\rho_{\text{eff}} = \rho(T_{\text{throat}}, P_{\text{ambient}}) \tag{49}$$

$$v_{\text{eff}} = a(T_{\text{throat}}, P_{\text{ambient}}) \tag{50}$$

Finally, Molkov et al. [42] specifies that mass and energy are conserved between the orifice and the notional nozzle and that the notional nozzle is at the speed of sound, i.e., Equation 42 along with the simultaneous solution of the equations,

$$\frac{v_{\text{eff}}^2}{2} + h(\rho_{\text{eff}}, P_{\text{ambient}}) = \frac{v_{\text{throat}}^2}{2} + h_{\text{throat}} \tag{51}$$

$$v_{\text{eff}} = a(\rho_{\text{eff}}, P_{\text{ambient}}) \tag{52}$$

where h and a are calculated using CoolProp [27].

To summarize, the 5 different notional nozzles available in HyRAM+ solve the equations:

- (default) Yüceil and Ötügen [38]: Equations 44, 45, and 46
- Birch et al. (1987) [39]: Equations 44, 45, and 47
- Birch et al. (1984) [40]: Equations 42, 47, and 48
- Ewan and Moody [41]: Equations 42, 49, and 50
- Molkov et al. [42]: Equations 42, 51, and 52

3.2.3. Initial Entrainment and Heating

The models in HyRAM+ are valid for hydrogen, methane, and propane, including saturated vapor and saturated liquid releases. Specifically for cryogenic hydrogen, as noted by Houf and Winters [43], there are challenges calculating properties in regions of the flow where oxygen and nitrogen from the entrained air would condense due to the extremely low temperatures. To account for this, conservation of mass, energy and momentum are applied until the temperature of the mixture (still assumed to be a plug-flow) is above a specified temperature (T_{min}). However, it should be noted that the default minimum temperature is 0 K, so this engineering model is unused in the GUI implementation. If the temperature of the notional nozzle (or at the orifice, if the flow is unchoked) is below T_{min}, the state after initial entrainment and heating is specified as hydrogen at T_{min}, and simultaneous solution to the momentum and energy balances yields the mass fraction of hydrogen (Y) when the mixture has warmed to T_{min}, i.e.,

$$\dot{m}_{\text{out}} = \dot{m}_{\text{in}} + \frac{1-Y}{Y}\dot{m}_{\text{in}} \tag{53}$$

$$v_{\text{out}} = v_{\text{in}}\frac{\dot{m}_{\text{in}}}{\dot{m}_{\text{out}}} \tag{54}$$

$$h_{\text{out}} = (1-Y)h_{\text{air}}(T_{min}, P_{\text{ambient}}) + Y h_{\text{H}_2}(T_{min}, P_{\text{ambient}}) + \frac{v_{\text{out}}^2}{2} \tag{55}$$

$$\dot{m}_{\text{out}}h_{\text{out}} = \dot{m}_{in}h_{\text{in}} + (\dot{m}_{\text{out}} - \dot{m}_{\text{in}})h_{\text{air}}(T_{\text{ambient}}, P_{\text{ambient}}) \tag{56}$$

Once the mass fraction (Y) is known, conservation of mass is used to yield the diameter of the plug flow at the end of the zone of initial entrainment and heating,

$$\rho_{\text{out}} = \frac{1}{\frac{1-Y}{\rho_{\text{air}}(T_{min},P_{\text{ambient}})} + \frac{Y}{\rho_{H_2}(T_{min},P_{\text{ambient}})}} \tag{57}$$

$$d_{\text{out}} = \sqrt{\frac{\pi \dot{m}_{\text{out}}}{4\rho_{\text{out}} v_{\text{out}}}} \tag{58}$$

and the momentum driven entrainment rate (see Equation 80) is used to calculate the length of this zone,

$$S = \frac{(1-Y)(\dot{m}_{\text{out}} - \dot{m}_{\text{in}})}{\rho_{\text{ambient}}(T_{\text{ambient}}, P_{\text{ambient}})E_{mom}} \tag{59}$$

3.2.4. Establishment of a Gaussian Profile

The flows described in Sections 3.2.1, 3.2.2, and 3.2.3 are all assumed to be plug flows, where the properties (e.g., velocity, density) are constant across the entire cross-section of the flow. However, jets, plumes, or flames from a pure source are well-known to have Gaussian profiles of their properties (e.g., velocity, density, mixture fraction) in the downstream regions [31, 44]. The final model for developing flow describes the transition from plug flow to the Gaussian profile that is used as an input to a one-dimensional system of ordinary differential equations that describes unignited dispersion or a diffusion flame (see Sections 3.3.1 and 3.4.2). Following the work of Winters [45], the centerline velocity of the Gaussian flow is assumed to be equivalent to the plug flow velocity, the jet is characterized by a half-width, B, where the velocity drops to half of the center-line value, and a spreading ratio, λ, the ratio of density spreading relative to velocity. The center-line (denoted with a cl subscript) mass-fraction is related to λ via the relationship,

$$\frac{\lambda^2+1}{2\lambda^2} = \frac{Y_{cl} - Y_{\text{ambient}}}{Y_{\text{plug}} - Y_{\text{ambient}}}. \tag{60}$$

Then the center-line molecular weight can be calculated,

$$\text{MW}_{cl} = \frac{1}{Y_{cl}/\text{MW}_{\text{C}_n\text{H}_{2n+2}} + (1-Y_{cl})/\text{MW}_{\text{air}}}. \tag{61}$$

The heat capacity of the fluid and ambient air are determined from CoolProp [27] and used to calculate the individual and mixture enthalpies as $h = c_p \cdot T$, where

$$c_{p,\text{plug}} = c_{p,\text{C}_n\text{H}_{2n+2}} Y_{\text{plug}} + c_{p,\text{air}}(1 - Y_{\text{plug}}), \tag{62}$$

$$c_{p,cl} = c_{p,\text{plug}} Y_{cl} + c_{p,\text{air}}(1 - Y_{cl}), \tag{63}$$

$$\frac{\lambda^2+1}{2\lambda^2} = \frac{h_{cl} - h_{\text{ambient}}}{h_{\text{plug}} - h_{\text{ambient}}}. \tag{64}$$

From these equations, the center-line temperature can be calculated, and the center-line density is calculated using the ideal gas equation of state, where

$$\rho_{cl} = \frac{\mathrm{MW}_{cl} P}{R T_{cl}}. \tag{65}$$

The length of the developing flow region is taken from Abraham [46], where $S/d = 6.2$, which assumes that the Froude number (Equation 84) is greater than the square root of 40 for these high speed, low density jets.

3.3. Unignited Releases

3.3.1. Gas Jet/Plume

For a jet or plume, HyRAM+ follows the one-dimensional model described by Houf and Winters [43]. While the model only considers one dimension, this dimension is along the streamline, and the jet/plume can curve due to buoyancy effects (or wind, although this aspect is not currently included). The reduction in dimension comes from the assumption that the mean profiles of the velocity (v), density (ρ), and product of density and mass fraction (Y) of fuel are Gaussian, as

$$v = v_{cl} \exp\left(-\frac{r^2}{B^2}\right) \tag{66}$$

$$\rho = (\rho_{cl} - \rho_{amb}) \exp\left(-\frac{r^2}{\lambda^2 B^2}\right) + \rho_{amb} \tag{67}$$

$$\rho Y = \rho_{cl} Y_{cl} \exp\left(-\frac{r^2}{\lambda^2 B^2}\right) \tag{68}$$

where B is a characteristic half-width, λ is the ratio of density spreading relative to velocity, the subscript *cl* denotes the centerline, the subscript *amb* denotes ambient, and r is perpendicular to the stream-wise direction. Gravity acts in the negative y-direction, and the plume angle, θ is relative to the x-axis (horizontal), as shown in Figure 3-3.

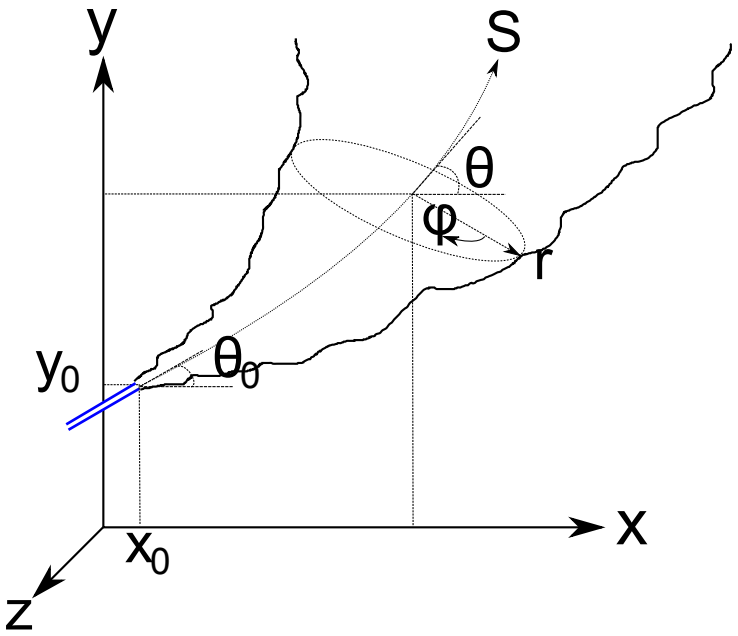

Figure 3-3 Sketch of plume model coordinates. Gravity acts in the negative y-direction.

The derivatives of the spatial dimensions are therefore

$$\frac{dx}{dS} = \cos\theta, \tag{69}$$

$$\frac{dy}{dS} = \sin\theta. \tag{70}$$

The conservation equations can be written as follows:

continuity:

$$\frac{d}{dS}\int_0^\infty (\rho v) 2\pi r dr = \rho_{amb} E, \tag{71}$$

x-momentum:

$$\frac{d}{dS}\int_0^\infty \left(\rho v^2 \cos\theta\right) 2\pi r dr = 0, \tag{72}$$

y-momentum:

$$\frac{d}{dS}\int_0^\infty \left(\rho v^2 \sin\theta\right) r dr = \int_0^\infty (\rho_{amb} - \rho) g r dr, \tag{73}$$

species continuity:

$$\frac{d}{dS}\int_0^\infty (\rho v Y) 2\pi r dr = 0, \tag{74}$$

energy:

$$\frac{d}{dS}\int_0^\infty \rho v\left(h+\frac{v^2}{2}-h_{amb}\right)2\pi r dr = 0. \tag{75}$$

Similar to Houf and Winters [43], HyRAM+ assumes that $h = c_p T$ and the ideal gas equation of state is used for these ambient pressure mixtures. The mixture molecular weight, heat capacity, and product of density and enthalpy all vary with respect to the radial coordinate (due to the fact that Y and ρ vary radially, see Equation 68) according to the following expressions:

$$\mathrm{MW} = \frac{\mathrm{MW}_{amb}\mathrm{MW}_{\mathrm{C}_n\mathrm{H}_{2n+2}}}{Y(\mathrm{MW}_{amb}-\mathrm{MW}_{\mathrm{C}_n\mathrm{H}_{2n+2}})+\mathrm{MW}_{\mathrm{C}_n\mathrm{H}_{2n+2}}}, \tag{76}$$

$$c_p = Y(c_{p,\mathrm{C_nH_{2n+2}}}-c_{p,amb})+c_{p,amb}, \tag{77}$$

$$\rho h = \frac{P}{c_p \mathrm{MW}}. \tag{78}$$

The Gaussian profiles in Equations 66-68 are plugged into the governing equations, and with the exception of the energy equation can be integrated analytically. For the energy equation, Equation 75, the numeric integration to infinity is estimated by evaluation to $5B$. This results in a system of 7 first order differential equations where the independent variable is S and the dependent variables are v_{cl}, B, ρ_{cl}, Y_{cl}, θ, x, and y. This system of equations is integrated from the starting point to the distance desired using an explicit Runge-Kutta method of order (4)5.

The entrainment model follows Houf and Schefer [44], where there is a combination of momentum and buoyancy driven entrainment,

$$E = E_{mom} + E_{buoy}, \tag{79}$$

where

$$E_{mom} = 0.282\left(\frac{\pi d_{\mathrm{exp}}^2}{4}\frac{\rho_{\mathrm{exp}} v_{\mathrm{exp}}^2}{\rho_\infty}\right)^{1/2}, \tag{80}$$

where the "exp" subscript denotes after the notional nozzle and zone of initial entrainment and heating (if used; see Sections 3.2.2 and 3.2.3), and

$$E_{buoy} = \frac{a}{\mathrm{Fr}_l}(2\pi v_{cl} B)\sin\theta, \tag{81}$$

where the local Froude number,

$$\mathrm{Fr}_l = \frac{v_{cl}^2}{gD(\rho_\infty-\rho_{cl})/\rho_{\mathrm{exit}}}. \tag{82}$$

In these equations, a is empirically determined:

$$\begin{cases} a = 17.313 - 0.116665\mathrm{Fr_{den}} + 2.0771\times10^{-4}\mathrm{Fr_{den}}^2, & \mathrm{Fr_{den}} < 268 \\ a = 0.97, & \mathrm{Fr_{den}} \geq 268, \end{cases} \tag{83}$$

with the densimetric Froude number

$$\mathrm{Fr}_{\mathrm{den}} = \frac{v_{\mathrm{plug}}}{\sqrt{g d_{\mathrm{plug}} |\rho_\infty - \rho_{\mathrm{plug}}| / \rho_{\mathrm{plug}}}}, \tag{84}$$

where the subscript "plug" denotes the plug flow at the exit of the orifice, notional nozzle, or zone of initial entrainment and heating, as applicable (see Sections 3.2.1, 3.2.2, and 3.2.3).

As the jet/plume becomes buoyancy-dominated (as opposed to momentum-dominated), the non-dimensional number

$$\alpha = \frac{E}{2\pi B v_{cl}} \tag{85}$$

will increase. When α reaches the limiting value of $\alpha = 0.082$, α is held constant and the entrainment value becomes:

$$E = 2\pi\alpha B v_{cl} = 0.164\pi B v_{cl}. \tag{86}$$

3.3.2. Tank Emptying

In the case of a storage tank with a given volume, the transient process of the tank emptying can also be calculated by HyRAM+. In this case, energy and mass are conserved, following the work of Hosseini et al. [47]. The mass flow rate, $\dot{m}$ is calculated as described in Section 3.2.1, whether the flow is choked or not. Energy is conserved in the tank volume, where

$$\frac{du}{dt} = \frac{\dot{m}(h-u)+q}{m}, \tag{87}$$

where u and h are the specific energy and specific enthalpy (J/kg), respectively, of the fuel in the tank (calculated using CoolProp [27]), m is the mass of fuel in the tank (kg), and q is the heat flow into the tank (J/s, $q = 0$ if adiabatic). This equation and the equations describing the mass flow rate (which are functions of the pressure and temperature inside the tank) are integrated until the mass or pressure in the tank reaches the desired stopping point (e.g., the tank pressure reaches ambient).

3.3.3. Accumulation in Confined Areas/Enclosures

When a release occurs in an enclosure, a stratified mixture of fuel and air can accumulate. For hydrogen or methane, the accumulated mixture will be near the ceiling due to buoyancy.

The release inside an enclosure is assumed to come from some tank with a fixed volume. Therefore, the flow from the tank follows Section 3.3.2. At each point in time for the blowdown, the jet/plume is modeled as described in Section 3.3.1. When these releases occur indoors, the plumes could impinge on a wall. Currently, should this impingement happen, the trajectory of the jet/plume is modified such that the fuel will travel vertically upwards along the wall, rather than in the horizontal direction, with the same features (e.g., half-width, centerline velocity). Note that this deflection upwards will occur regardless of the fuel and is a poor assumption for heavier fuels such as propane.

Accumulation occurs following the model of Lowesmith et al. [48], where a layer forms along the ceiling. Conservation of mass requires that

$$\frac{dV_l}{dt} = Q_{\text{in}} - Q_{\text{out}}, \tag{88}$$

where V_l is the volume of gas in the layer, and Q is the volumetric flow rate, with subscript "in" referring to the flow rate of fuel and air entrained into the jet at the height of the layer, and "out" referring to flow out the ventilation. Species conservation requires that

$$\frac{d(\chi V_l)}{dt} = Q_{\text{leak}} - \chi Q_{\text{out}}, \tag{89}$$

where χ is the mole or volume fraction of fuel in the layer and Q_{leak} is the leak rate of the fuel. Expanding the derivative and substituting Equation 88 yields

$$V_l \frac{d\chi}{dt} = Q_{\text{leak}} - \chi Q_{\text{in}}. \tag{90}$$

Q_{in} is solved for by modeling a jet/plume within the enclosure to calculate the jet half-width (B) and centerline velocity (v_{cl}), as described in Section 3.3.1 at the height of the bottom of the layer. The volumetric flow rate (Q_{in}) is calculated as:

$$Q_{\text{in}} = \pi B^2 v_{cl}. \tag{91}$$

Flows out of the enclosure are driven by buoyancy, and potentially wind or a fan. Buoyancy driven flow is calculated as

$$Q_b = C_d A_v \sqrt{g' H_l}, \tag{92}$$

where C_d is a coefficient of discharge, A_v is the area of the upper (outlet) vent, H_l is the height of the layer (between the bottom of the layer and the center-point of the outlet vent), and g' is reduced gravity:

$$g' = g \frac{\rho_{\text{air}} - \rho_l}{\rho_{\text{air}}}, \tag{93}$$

where g is the gravitational constant, ρ_l is the density of the layer, and ρ_{air} is the density of air (at the temperature and pressure of the enclosure). The density in the layer (ρ_l) is calculated from the density of air (ρ_{air}) and the density of the fuel ($\rho_{C_nH_{2n+2}}$), both at the temperature and pressure of the enclosure, as:

$$\rho_l = \chi \rho_{C_nH_{2n+2}} + (1-\chi)\rho_{\text{air}}. \tag{94}$$

Wind (or mechanical ventilation) is assumed to drive the flow at a rate of:

$$Q_w = \frac{C_d A_v U_w}{\sqrt{2}} = \frac{C_d Q_{\text{vent}}}{\sqrt{2}}, \tag{95}$$

where C_d is a coefficient of discharge, A_v is the area of the lower (inlet) vent, U_w is the velocity of the wind (or mechanical ventilation) through the lower (inlet) vent, and Q_{vent} is the volumetric flow rate through the lower (inlet) vent ($Q_{\text{vent}} = A_v U_w$). Note that Q_{vent} is a user input.

The total flow out of the enclosure, accounting for buoyancy driven flow and flow from the vent, is calculated as

$$Q_{\text{out}} = Q_{\text{leak}} + \sqrt{Q_b^2 + Q_w^2}. \tag{96}$$

3.4. Ignited Releases

3.4.1. Flame Correlations

As noted by Houf and Schefer [49], a non-dimensional flame length, defined as

$$L^* = \frac{L_{\text{vis}} f_s}{d_j \sqrt{\rho_j / \rho_{amb}}} \tag{97}$$

collapses onto a single curve for a range of fuels (hydrogen, methane, and propane), where L_{vis} is the visible flame length (from the orifice, including any liftoff distance), f_s is the mass fraction of fuel in a stoichiometric mixture of fuel and air (Equation 35), and d_j, ρ_j, and ρ_{amb} are the orifice diameter, density of fuel at the orifice, and density of air, respectively. The curve is given by

$$L^* = \begin{cases} \frac{13.5\text{Fr}^{2/5}}{(1+0.07\text{Fr}^2)^{1/5}}, & \text{Fr} < 5, \\ 23, & \text{Fr} > 5, \end{cases} \tag{98}$$

which is a function of the Froude number (Fr), which is the ratio of buoyancy to momentum forces. The Froude number is defined as

$$\text{Fr} = \frac{u_j f_s^{3/2}}{\sqrt{g d_j (T_{\text{ad}} - T_{amb})/T_{amb} \sqrt{\rho_j / \rho_{amb}}}}, \tag{99}$$

where g is the gravitational constant, u_j is the velocity of the jet at the orifice, T_{ad} is the adiabatic flame temperature (for a stoichiometric mixture, see section 3.1.2), and T_{amb} is the ambient temperature. The flame width is constant at $W_f = 0.17 L_{\text{vis}}$ [50, 51].

The total emitted radiative power from a flame, S_{rad}, is related to the total energy in the flame by the radiant fraction,

$$S_{\text{rad}} = X_{\text{rad}} \dot{m}_{\text{fuel}} \Delta H_c, \tag{100}$$

where X_{rad} is the radiant fraction, $\dot{m}_{\text{fuel}}$ is the mass flow rate of fuel, and ΔH_c is the heat of combustion (120 MJ/kg for hydrogen, 50 MJ/kg for methane, and 46.4 MJ/kg for propane [33, 34]). The radiant fraction (X_{rad}) varies with the flame residence time (τ_f); the relationship is [52]

$$X_{\text{rad}} = 9.45 \times 10^{-9} (\tau_f a_p T_{\text{ad}}^4)^{0.47}, \tag{101}$$

where a_p is the Planck-mean absorption coefficient for an optically thin flame (0.23 for hydrogen [53]). The Plank-mean absorption coefficient should be updated for methane and propane, but the current value of 0.23 is used for all fuels. The flame residence time can be calculated as

$$\tau_f = \frac{\rho_f W_f^2 L_{\text{vis}} f_s}{3 \rho_j d_j^2 u_j}, \tag{102}$$

where ρ_f is the flame density. The flame density is calculated as the density at the adiabatic flame temperature:

$$\rho_f = \frac{p_{amb} W_{\text{mix}}}{R T_{\text{ad}}}, \tag{103}$$

where p_{amb} is the ambient pressure, W_{mix} is the mean molecular weight of the stoichiometric products of combustion in air, and R is the universal gas constant.

The transmissivity, which can reduce the radiated heat flux is calculated to account for the absorption from water vapor and CO_2, using a correlation from Wayne [54]:

$$\begin{aligned}\tau = 1.006 &- 0.001171\left(\log_{10} X_{\text{H}_2\text{O}}\right) - 0.02368\left(\log_{10} X_{\text{H}_2\text{O}}\right)^2 \\ &- 0.03188\left(\log_{10} X_{\text{CO}_2}\right) + 0.001164\left(\log_{10} X_{\text{CO}_2}\right)^2,\end{aligned} \tag{104}$$

where $X_{\text{H}_2\text{O}}$ and X_{CO_2} is proportional to the amount of water vapor or CO_2 in the path (dimensionless). These values are calculated by:

$$X_{\text{CO}_2} = L \cdot \frac{273}{T} \cdot \frac{c_{\text{CO}_2}}{335}, \tag{105}$$

$$X_{\text{H}_2\text{O}} = R_H \cdot L \cdot S_{\text{mm}} \cdot \frac{2.88651 \times 10^2}{T}. \tag{106}$$

In these relationships, L is the path length (m) through which the radiative light must travel, T is the ambient temperature (K), c_{CO_2} is the concentration of CO_2 in the atmosphere (ppm, assumed to be 400 ppm), R_H is the fractional relative humidity (ranges from 0–1), and S_{mm} is the saturated water vapor pressure (mm Hg), estimated by the relationship:

$$S_{\text{mm}} = \exp\left(10.386 - \frac{5132}{T}\right). \tag{107}$$

3.4.2. Jet Flame with Buoyancy Correction

A similar model to the jet/plume model described in Section 3.3.1 is also used to describe a flame. The model is described by Ekoto et al. [31]. The major difference between the jet/plume model and the flame model is that rather than the mole fraction, the mixture fraction, shown in Equation 37, is a conserved scalar. Similar assumptions are made for Gaussian profiles of the velocity and mixture fraction:

$$v = v_{cl} \exp\left(-\frac{r^2}{B^2}\right), \tag{108}$$

$$f = f_{cl} \exp\left(-\frac{r^2}{\lambda^2 B^2}\right), \tag{109}$$

with the conservation equations written as

x-centerline:

$$\frac{dx}{dS} = \cos\theta, \tag{110}$$

y-centerline:

$$\frac{dy}{dS} = \sin\theta, \tag{111}$$

continuity:

$$\frac{d}{dS} 2\pi \int_0^\infty \rho v r dr = \rho_{amb} E, \tag{112}$$

x-momentum:

$$\frac{d}{dS} 2\pi \int_0^\infty \rho v^2 \cos\theta r dr = \rho_{amb} E v_{\text{wind}}, \tag{113}$$

y-momentum:

$$\frac{d}{dS} \int_0^\infty \rho v^2 \sin\theta r dr = \int_0^\infty (\rho_{amb} - \rho) g r dr, \tag{114}$$

mixture fraction:

$$\frac{d}{dS} 2\pi \int_0^\infty \rho V f r dr = 0. \tag{115}$$

Note that energy conservation is not included in this formulation, but rather the mixture is assumed to be thermally perfect, with combustion calculations shown in Section 3.1.2. These calculations assume that the mixture is always in equilibrium (neglecting heat-losses), which results in a calculation of flame temperature and density as functions of mixture fraction similar to Figure 3-2 (with slight variations depending on the reactant temperature).

Equation 113 does not explicitly set the right-hand side of the x-momentum equation to 0, as is done in the unignited jet/plume model (Equation 72). While the Windows GUI version of HyRAM+ sets $v_{\text{wind}} = 0$, the Python backend enables specification of a cross-wind velocity, v_{wind}. The Gaussian profiles in Equations 108 and 109 are numerically evaluated out to $5B$ (an estimate of ∞), along with the radial profiles of the density (based off of the mixture fraction), which can be plugged into Equations 110–115 and numerically integrated. This results in a system of 6 first order differential equations where the independent variable is S and the dependent variables are v_{cl}, B, θ, f_{cl}, x, and y. This system of equations is integrated from the starting point to the distance desired using an Adams/BDF method with automatic stiffness detection and switching. Typically, the integration distance is the visible flame length, calculated using the correlations in Equations 97 and 98.

Similar to the nonreacting jet, entrainment in the jet flame is modeled as the sum of momentum and buoyancy contributions (Equation 79). However, rather than defining the buoyancy caused entrainment as before (Equation 81), buoyancy driven entrainment is calculated as

$$E_{buoy} = 2\pi\alpha_{buoy} g \sin\theta \frac{\int_0^\infty (\rho_{amb} - \rho) dr}{B v_{cl} \rho_{exit}}. \tag{116}$$

The empirical constant for momentum driven entrianment in Equation 80 of 0.282, and empirical constant for buoyancy driven entrainment in Equation 116 (α_{buoy}) are also different for flames rather than unignited plumes/jets, with a value of 0.0342 for momentum driven entrainment, and $\alpha_{buoy} = 5.75 \times 10^{-4}$ [31].

3.4.3. Radiation From a Curved Flame

The radiative heat flux from the buoyancy corrected, curved flame is calculated by a weighted multi-source model, similar to that described by Hankinson and Lowesmith [55]. The heat flux at a point along the flame is calculated as

$$q = \tau S_{\text{rad}} \frac{V_F}{A_f}, \tag{117}$$

where S_{rad} is calculated according to Equations 100–102, V_F is the view-factor, proportional to the heat flux transmitted to the observer, τ is the transmissivity, calculated by Equation 104, and A_f is the surface area of the flame. Contributions to the total heat flux are broken up into many (N, generally 50) points along the length of the curved flame, and the weighted average proceeds as

$$\tau \frac{V_F}{A_f} = \sum_{i=1}^{N} \frac{w_i \cos \beta_i}{4\pi D_i^2} \tau_i, \tag{118}$$

where the emitter strength weighting parameter

$$w_i = \begin{cases} i w_1 & i \leq 0.75N \\ \left[n - \frac{n-1}{N-n-1} (i - (n+1)) \right] w_1 & i > 0.75N, \end{cases} \tag{119}$$

with the constraint that $1 \leq n \leq N$ and $\sum_{i=1}^{N} w_i = 1$. In these equations, D and β are the distance and angle, respectively between the observer and unit normal to the point emitter.

3.4.4. Overpressure in Enclosures

If a confined mixture ignites, significant overpressures can develop within the enclosure or confinement area. Overpressure is calculated assuming that the cause of overpressure is the volume change on combustion pressurizing the enclosure. Within HyRAM+, the models described in Section 3.3.3 are used to calculate the volume of fuel within the layer and entire enclosure. It is assumed that all of the fuel within the flammability limits (in both the jet/plume and the accumulated layer) reacts, and the overpressure is calculated, following Bauwens and Dorofeev [56] as

$$\Delta p = p_0 \left(\left[\left(\frac{V_T + V_{\text{C}_\text{n}\text{H}_{2\text{n}+2}}}{V_T} \right) \left(\frac{V_T + V_{\text{stoich}} (\sigma - 1)}{V_T} \right) \right]^{\gamma} - 1 \right), \tag{120}$$

where p_0 is the initial pressure, V_T is the total volume of the enclosure, $V_{\text{C}_\text{n}\text{H}_{2\text{n}+2}}$ is the expanded volume of pure fuel following the release, V_{stoich} is the volume of a stoichiometric mixture of the consumed fuel, σ is the expansion ratio of a stoichiometric fuel-air mixture, and γ is the specific heat ratio of air. The expanded volume is given by $V_{\text{C}_\text{n}\text{H}_{2\text{n}+2}} = m_{\text{C}_\text{n}\text{H}_{2\text{n}+2}} / \rho_{\text{C}_\text{n}\text{H}_{2\text{n}+2}}$ where $m_{\text{C}_\text{n}\text{H}_{2\text{n}+2}}$ is the mass of fuel consumed and $\rho_{\text{C}_\text{n}\text{H}_{2\text{n}+2}}$ is the density of the fuel at ambient conditions. V_{stoich} is $V_{\text{C}_\text{n}\text{H}_{2\text{n}+2}}$ divided by the stoichiometric mole fraction of fuel.

3.4.5. Unconfined Overpressure

If an unconfined mixture ignites after a release has been flowing for some time, overpressures can be observed as the initial mixture burns. HyRAM+ has three different methods for calculating the overpressure. Each of these methods requires the calculations from an unconfined, unignited jet/plume, as described in Section 3.3.1. Each method calculates an overpressure and possibly impulse as a function of distance, R. We assume that the origin for the overpressure/impulse (distance from which R is measured) is the point at which the fuel concentration is halfway between the lower and upper flammability limits along the jet streamline[7]. This is assumed to be a reasonable origin location, given the overpressure blast wave will originate from the flammable mixture.[8].

BST The Baker-Strehlow-Tang (BST) model is based on blast curves that relate overpressure and impulse to the Mach flame speed [58]. The flammable mass of fuel within the unignited jet/plume (m_{flam}) is first found by volumetrically integrating the product of the mass fraction (Y) and density (ρ) of the jet/plume that is within the flammability limits (Y_{LFL}, Y_{UFL}) along the entire length of the jet/plume streamline coordinate (S), or

$$m_{\mathrm{flam}} = \int_{S=0}^{S=\infty} \left(\int_{r_{Y=Y_{\mathrm{UFL}}}}^{r_{Y=Y_{\mathrm{LFL}}}} \rho Y 2\pi r dr \right) dS. \tag{121}$$

The energy within the unignited flammable mixture (E_{flam}) is related to the flammable mass through the relationship

$$E_{\mathrm{flam}} = k_{\mathrm{reflection}} m_{\mathrm{flam}} \Delta H_c \tag{122}$$

where $k_{\mathrm{reflection}}$ is a ground reflection factor (assumed to be 2) and ΔH_c is the heat of combustion of the fuel [58]. The scaled distance is related to the energy through the relationship [58]

$$R^*_{\mathrm{BST}} = \frac{R}{(E_{\mathrm{flam}}/P_{\mathrm{ambient}})^{1/3}}. \tag{123}$$

The scaled overpressure and impulse are related to the scaled distance, based on the Mach flame speed, as shown in Figure 3-4 [58].

[7]Note that is different than in HyRAM+ version 4.0 [1], for which the overpressure/impulse origin was $1/2$ the distance to the lower flammability limit along the jet centerline

[8]This is also roughly consistant with the suggested ignition conentration by Jallais et al. [57] for hydrogen.

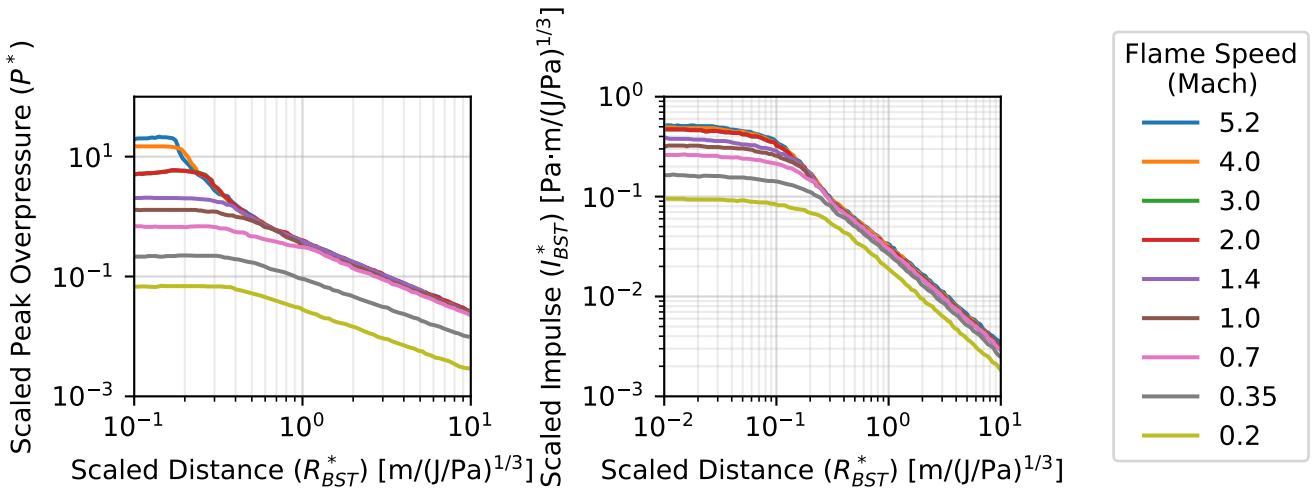

Figure 3-4 Mapping of scaled distance to scaled overpressure (top) and scaled impulse (bottom) for the BST unconfined overpressure model [1].

The scaled overpressure (P^*) is the peak overpressure (P_s) relative to ambient pressure (P_{ambient}),

$$P^* = P_s / P_{\text{ambient}}, \tag{124}$$

and the impulse (I) is scaled by the flammable energy (E_{flam}), ambient pressure (P_{ambient}), and speed of sound for air ($a_{\text{air}} = 340$ m/s) as

$$I^*_{\text{BST}} = \frac{I a_{\text{air}}}{(E_{\text{flam}} P^2_{\text{ambient}})^{1/3}}. \tag{125}$$

TNT The TNT equivalence method is based on finding the mass of TNT that contains the same energy as the fuel being combusted [58]. The flammable mass of fuel within the jet/plume (m_{flam}) is found by volumetrically integrating the product of the mass fraction and density of the jet/plume that is within the flammability limits (see Equation 121). The flammable mass is scaled by an equivalence factor (F_{equiv}), 3% by default [58]), and the equivalent mass of TNT ($m_{TNT_{equiv}}$) is calculated as

$$m_{\text{TNT}_{\text{equiv}}} = F_{\text{equiv}} \frac{m_{\text{flam}} \Delta H_c}{\Delta H_{c,\text{TNT}}}, \tag{126}$$

where and $\Delta H_{c,\text{TNT}} = 4.68$ MJ/kg is the equivalent specific blast energy of TNT. The scaled distance (R^*_{TNT}) is related to the equivalent mass of TNT ($m_{\text{TNT}_{\text{equiv}}}$) through the relationship

$$R^*_{\text{TNT}} = \frac{R}{m^{1/3}_{\text{TNT}_{\text{equiv}}}}, \tag{127}$$

and the scaled overpressure (P^*) and scaled impulse (I^*_{TNT}) resulting from combustion are related to the scaled distance as shown by Figure 3-5.

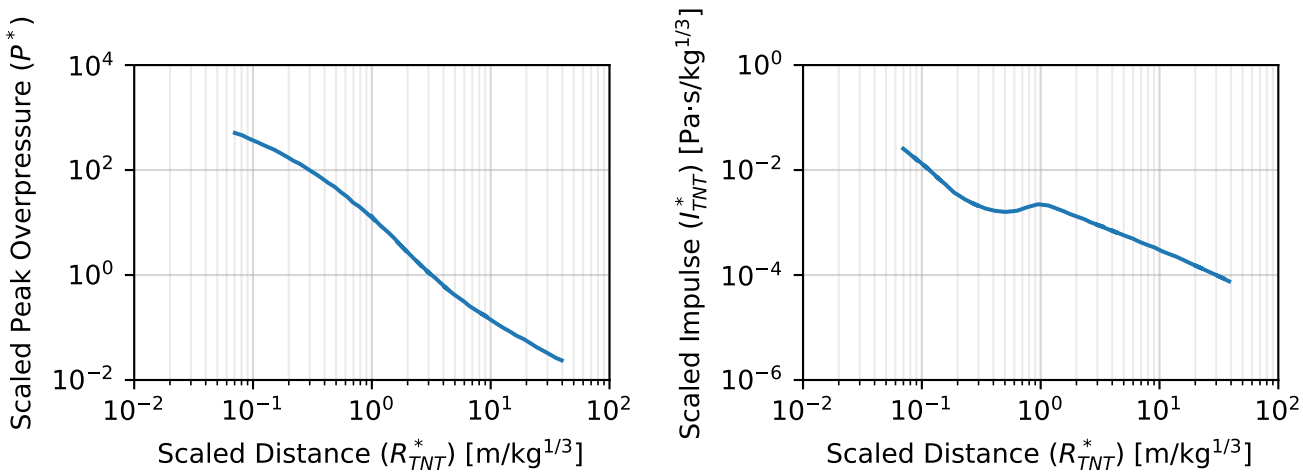

Figure 3-5 Mapping of scaled distance to scaled overpressure (top) and scaled impulse (bottom) for the TNT equivalence unconfined overpressure model [1].

The scaled overpressure (P^*) is the overpressure (P_s) relative to ambient pressure (see Equation 124), and the impulse (I) is scaled by the third root of the TNT mass ($m_{\mathrm{TNT_{equiv}}}$), or

$$I^*_{\mathrm{TNT}} = \frac{I}{m^{1/3}_{\mathrm{TNT_{equiv}}}}. \tag{128}$$

Bauwens The Bauwens method for unconfined overpressure calcuation is based on the work of Bauwens and Dorfeev [59, 60]. In this method, the detonable mass within the unconfined jet/plume is calculated and then the overpressure is based on detonation of that mass of fuel.

The detonation cell size (λ_{det}) is calculated at each point in the jet/plume, based on the mass fraction field (Y, see section 3.3.1) and fits to data from the detonation database [61]. The fits to the data are based on a polynomial fit in log-log space:

$$\ln\lambda_{det} = a + b\ln\phi + c(\ln\phi)^2 + d(\ln\phi)^3 + e(\ln\phi)^4, \tag{129}$$

where the parameters a–e are given in Table 3-1[9].

Table 3-1 Detonation cell size fitted parameters

Fuel	a	b	c	d	e
H_2	2.94771698	-0.16536739	2.2608031	-1.18064551	0.45823461
CH_4	5.768321	1.13938677	113.36802963	0	0
C_3H_8	4.44856885	-0.73108257	5.50526263	0	0

The fits and data for different fuels are shown in Figure 3-6.

[9]Note that these fits are slightly different than the previously used fits in HyRAM+ version 4.0 [1]

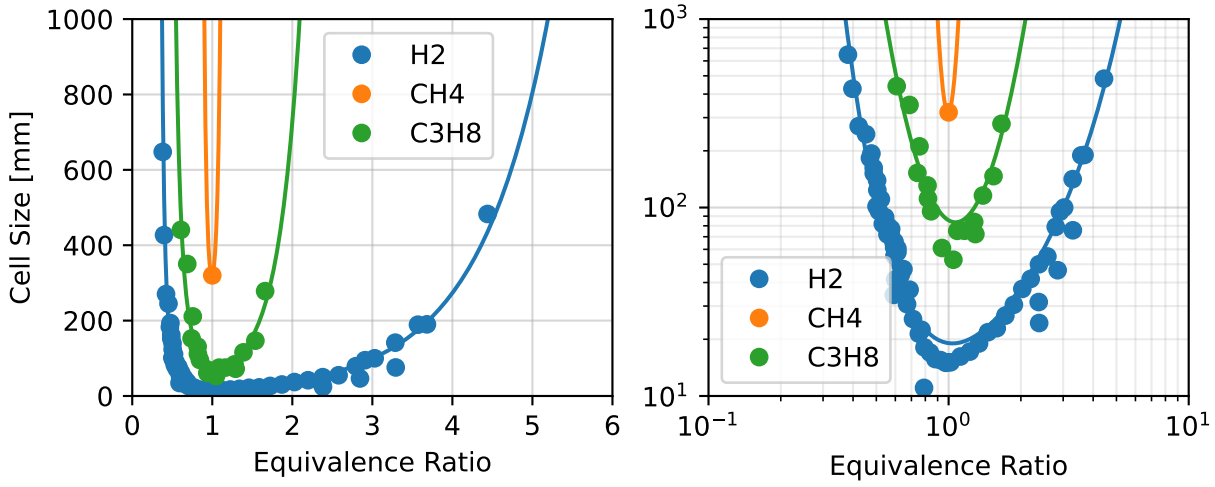

Figure 3-6 Detonation cell size data (points) from the detonation database [61] and fits to the data (lines) on a linear (left) and logarithmic (right) scale.

Once the detonation cell size is calculated, the gradient in the radial direction of the detonation cell size ($d\lambda_{det}/dr$) is found numerically. In addition, the number of cells that fit within the layer ($n_{\lambda_{det}}$) is numerically calculated as

$$n_{\lambda_{det}} = \int_0^r \frac{dr}{\lambda_{det}(r)}. \tag{130}$$

Detonations are presumed to propagate in areas that are within the flammability limits, with a detonation cell size gradient less than 0.1 ($d\lambda_{det}/dr < 0.1$), and where there are at least 5 cells within the layer ($n_{\lambda_{det}} \geq 5$). The mass of fuel within the jet/plume that meets these constraints is calculated as the detonable mass (m_{det}). In equation form,

$$m_{\text{det}} = \int_{S=0}^{\infty} \left(\int_{r=0}^{\infty} \rho Y 2\pi r dr \right) dS, \quad \text{where } Y_{\text{lean}} \leq Y \leq Y_{\text{rich}},\ d\lambda_{det}/dr < 0.1, \text{ and } n_{\lambda_{det}} \geq 5. \tag{131}$$

The dimensionless distance (R^*_{Bauwens}) from the center of the detonable region is calculated as

$$R^*_{\text{Bauwens}} = R \left(\frac{P_{\text{ambient}}}{E_{\text{det}}} \right)^{1/3}, \tag{132}$$

where the energy of detonable fuel (E_{det}) is calculated as

$$E_{\text{det}} = m_{\text{det}} \Delta H_c. \tag{133}$$

Finally, the scaled overpressure (P^*) is calculated as

$$P^* = \frac{0.34}{(R^*)^{4/3}} + \frac{0.062}{(R^*)^2} + \frac{0.0033}{(R^*)^3}. \tag{134}$$

There is currently no calculation of impulse for this model. This means that the overpressure probit models in Section 2.6.2 that use impulse cannot be used with this model.

This page intentionally left blank.

4. ENGINEERING TOOLKIT

This section describes the Engineering Toolkit, which uses the models described elsewhere in this report to perform simple calculations for properties of the different fuels.

4.1. Temperature, Pressure, and Density

The user can calculate one of the quantities temperature (T), pressure (P), or density (ρ) by specifying the other two. For saturated liquid or saturated vapor phases, only one of the temperature, pressure, or density need to be specified, the other two will be calculated. The algorithm uses the CoolProp library [27] to perform the thermodynamic calculations (see Section 3.1.1).

4.2. Tank Mass

The user can calculate the mass (m) of fuel in a container by specifying the temperature, pressure, and volume (V) of the container using Equation 135. The density of the fuel (ρ) is calculated using the specified temperature and pressure using the CoolProp library [27] as described in Section 4.1.

$$m = \rho V \tag{135}$$

4.3. Mass Flow Rate

The mass flow rate of a leak from a tank can be calculated for either a steady release or for a pressure blowdown of a tank. A "blowdown" describes the release of gas from a tank until the pressure reaches ambient, causing the mass flow to stop. This can be estimated from the temperature, pressure, and leak size for a steady release, and also volume for a blowdown case.

For a steady-state release, the mass flow rate ($\dot{m}$) is calculated using the density of the fluid (ρ), the velocity of the fluid through the orifice (v), and the area of the orifice (A) using Equation 136.

$$\dot{m} = \rho v A \tag{136}$$

The area of the orifice is given by the diameter of the orifice (d) and is calculated using Equation 9[10]. The density (ρ) and velocity (v) of the fluid depend on the temperature and pressure of the tank and are calculated for the flowing fluid as described in Section 3.2.1. The output for the steady state case is the mass flow rate in kg/s.

For the blowdown case, the initial mass in the tank (m_0) is calculated (same as Section 4.2) using Equation 137, where ρ_0 is the initial density of hydrogen in the tank (which depends on the initial

[10]The discharge coefficient for the Engineering Toolkit is assumed to be equal to 1.0.

temperature and pressure of the tank and is calculated as described in Section 4.1) and V is the volume of the tank.

$$m_0 = \rho_0 V \tag{137}$$

The mass and energy flow equations (as described in Section 3.3.2) are then integrated until the the tank pressure is equal to ambient pressure (101,325 Pa)[11]. The output for the blowdown case is a combination plot of the mass in the tank, tank pressure, mass flow rate, and temperature over time, as well as the total time needed for the tank to empty in seconds.

4.4. TNT Mass Equivalence

The TNT mass equivalence ($m_{\text{TNT equivalent}}$) can be calculated using Equation 138 with the flammable vapor release mass (m_{fuel}), the explosive energy yield (Y, 0–100%), and the net heat of combustion (ΔH_c).

$$m_{\text{TNT equivalent}} = \frac{m_{\text{fuel}} \times Y \times \Delta H_c}{4500 \text{ kJ/kg}_{\text{TNT}}} \tag{138}$$

The heat of combustion for hydrogen, methane, and propane are $\Delta H_{c,\text{ hydrogen}} = 120$ MJ/kg, $\Delta H_{c,\text{ methane}} = 50.0$ MJ/kg, $\Delta H_{c,\text{ propane}} = 46.4$ MJ/kg [33, 34]. The TNT mass equivalence equation and 4,500 kJ/kg$_{\text{TNT}}$ equivalnce factor used are from NUREG-1805 [62].

[11] The ending/ambient pressure for the Engineering Toolkit Mass Flow Rate Blowdown calculations is set to be 101,325 Pa, the ambient pressure at sea level. Future versions of HyRAM+ may allow the ending/ambient pressure to be specified in this calculation

5. SUMMARY OF NUMERICAL METHODS

5.1. Python Calculation Methods

The Python modules in HyRAM+ utilize the NumPy and SciPy packages [63–65]. NumPy provides support for multi-dimensional arrays, mathematical functions of arrays, and some numerical linear algebra routines. SciPy provides a variety of numerical method routines including support for statistical distributions, numerical linear algebra, integration, interpolation, optimization, root-finding, ordinary differential equation solvers, and others. Plots in HyRAM+ are made using Matplotlib [66].

5.2. Leak Frequency Computations

Almost all of the computations for HyRAM+ are done in the Python code modules. However, the HyRAM+ QRA mode uses statistical distributions from Math.NET [67] for calculating the component release frequency mean and variance (see Section 2.4). This allows the leak frequency values to update quickly in the front-end without calling Python.

5.3. Unit Conversion

HyRAM+ enforces an immutable link between values and the units that define them. Input values are stored in the International System of Units (SI). Conversions are performed implicitly by the system. Therefore, the application is able to present data in units preferred by the user or more relevant in problem context, while being able to pass data to the Python calculation algorithms in the expected SI units. Table 5-1 contains the convertible units currently available in HyRAM+. Note that all pressure units are assumed to be absolute pressure, not gauge pressure.

Table 5-1 HyRAM+ convertible units.

Unit Type	Units Available
Distance	m, cm, mm, in, ft, yd, mi, au
Area	m^2, cm^2, mm^2, ft^2, in^2, yd^2
Volume	cm^3, dm^3, dam^3, m^3, km^3, mm^3, μm^3, ft^3, in^3, yd^3, mi^3, L, μL, mL, dL, daL, kL, ML
Angle	radians, degrees
Energy	J, kWh, BTU
Time	s, ms, min, hr
Pressure	Pa, kPa, MPa, psi, atm, bar, J/m^3
Temperature	Celsius, Fahrenheit, Kelvin
Speed	m/s
Volumetric Flow Rate	m^3/s

This page intentionally left blank.

REFERENCES

[1] E. S. Hecht, B. D. Ehrhart, K. M. Groth, J. T. Reynolds, M. L. Blaylock, and E. E. Carrier, "Hydrogen Plus Other Alternative Fuels Risk Assessment Models (HyRAM+) Version 4.0 Technical Reference Manual," Tech. Rep. SAND2021-14813, Sandia National Laboratories, November 2021.

[2] B. D. Ehrhart, E. S. Hecht, K. M. Groth, J. T. Reynolds, M. L. Blaylock, and E. E. Carrier, "Hydrogen Risk Assessment Models (HyRAM) Version 3.1 Technical Reference Manual," Tech. Rep. SAND2021-5812, Sandia National Laboratories, May 2021.

[3] B. D. Ehrhart, E. S. Hecht, K. M. Groth, J. T. Reynolds, M. L. Blaylock, and E. E. Carrier, "Hydrogen Risk Assessment Models (HyRAM) Version 3.0 Technical Reference Manual," Tech. Rep. SAND2020-10600, Sandia National Laboratories, September 2020.

[4] K. M. Groth, E. S. Hecht, J. T. Reynolds, M. L. Blaylock, and E. E. Carrier, "Methodology for assessing the safety of Hydrogen Systems: HyRAM 1.1 technical reference manual," Tech. Rep. SAND2017-2998, Sandia National Laboratories, March 2017.

[5] K. M. Groth, E. S. Hecht, and J. T. Reynolds, "Methodology for assessing the safety of Hydrogen Systems: HyRAM 1.0 technical reference manual," Tech. Rep. SAND2015-10216, Sandia National Laboratories, November 2015.

[6] K. M. Groth and A. V. Tchouvelev, "A toolkit for integrated deterministic and probabilistic assessment for hydrogen infrastructure," in *Proceedings of the Probabilistic Safety and Management Conference (PSAM 12)*, (Honolulu, HI (USA)), June 22-27 2014.

[7] K. M. Groth and E. S. Hecht, "HyRAM: a methodology and toolkit for quantitative risk assessment of hydrogen systems," in *Proceedings of the International Conference on Hydrogen Safety (ICHS 2015)*, (Yokohama (Japan)), October 19-21 2015.

[8] K. M. Groth and E. S. Hecht, "HyRAM: A methodology and toolkit for quantitative risk assessment of hydrogen systems," *International Journal of Hydrogen Energy*, vol. 42, no. 11, pp. 7485–7493, 2017.

[9] B. D. Ehrhart, E. S. Hecht, and J. A. Mohmand, "Validation and comparison of HyRAM physics models," Tech. Rep. SAND2021-5811, Sandia National Laboratories, May 2021.

[10] S. Egbert, X. Li, M. L. Blaylock, and E. Hecht, "Mixing of liquid methane releases.," Tech. Rep. SAND2018-13757R, Sandia National Laboratories, 2018.

[11] M. L. Blaylock, E. Hecht, and C. Jordan, "Validation of the altram physics models for use with compressed natural gas," Tech. Rep. SAND2019-13408, Sandia National Laboratories, June 2020.

[12] J. G. Shum, E. S. Hecht, and M. L. Blaylock, "Validation of the HyRAM+ physics models for use with propane," Tech. Rep. SAND2021-3244, Sandia National Laboratories, 2021.

[13] K. M. Groth, J. L. LaChance, and A. P. Harris, "Early-stage quantitative risk assessment to support development of codes and standard requirements for indoor fueling of hydrogen vehicles," Tech. Rep. SAND2012-10150, Sandia National Laboratories, November 2012.

[14] A. V. Tchouvelev, "Knowledge gaps in hydrogen safety: A white paper," tech. rep., International Energy Agency Hydrogen Implementing Agreement Task 19, January 2008.

[15] J. LaChance, W. Houf, B. Middleton, and L. Fluer, "Analyses to support development of risk-informed separation distances for hydrogen codes and standards," Tech. Rep. SAND2009-0874, Sandia National Laboratories, March 2009.

[16] A. Glover, A. Baird, and D. Brooks, "Final report on hydrogen planthazards and risk analysissupporting hydrogen plant sitingnear nuclear power plants," Tech. Rep. SAND2020-7946, Sandia National Laboratories, July 2020.

[17] D. M. Brooks, B. D. Ehrhart, and C. LaFleur, "Development of liquid hydrogen leak frequencies using a Bayesian update process," in *2021 International Conference on Hydrogen Safety*, September 2021.

[18] G. W. Mulcahy, D. M. Brooks, and B. D. Ehrhart, "Using Bayesian methodology to estimate liquefied natural gas leak frequencies," Tech. Rep. SAND2021-4905, Sandia National Laboratories, April 2021.

[19] N. A. Eisenberg, C. J. Lynch, and R. J. Breeding, "Vulnerability model. A simulation system for assessing damage resulting from marine spills," Tech. Rep. SA/A-015 245, U.S. Coast Guard, 1975.

[20] C. K. Tsao and W. W. Perry, "Modifications to the vulnerability model: a simulation system for assessing damage resulting from marine spills," Tech. Rep. ADA 075 231, U.S. Coast Guard, 1979.

[21] TNO, "Methods for the determination of possible damage," Tech. Rep. CPR 16E, The Netherlands Organization of Applied Scientific Research (TNO), 1992.

[22] F. P. Lees, "The assessment of major hazards: a model for fatal injury from burns," *Process Safety and Environmental Protection*, vol. 72, no. 3, pp. 127–134, 1994.

[23] J. LaChance, A. Tchouvelev, and A. Engebø, "Development of uniform harm criteria for use in quantitative risk analysis of the hydrogen infrastructure," *International Journal of Hydrogen Energy*, vol. 36, pp. 2381–2388, February 2011.

[24] Center for Chemical Process Safety (CCPS), *Guidelines for Chemical Process Quantitative Risk Analysis*. American Institute of Chemical Engineers, 1999.

[25] HSE, *Major hazard aspects of the transport of dangerous substances*. UK Health and Safety Executive, 1991.

[26] UK Health and Safety Executive, "Methods of approximation and determination of human vulnerability for offshore major accident hazard assessment," tech. rep., UK Health and Safety Executive, 2010.

[27] I. H. Bell, J. Wronski, S. Quoilin, and V. Lemort, "Pure and Pseudo-pure Fluid Thermophysical Property Evaluation and the Open-Source Thermophysical Property Library CoolProp," *Industrial & Engineering Chemistry Research*, vol. 53, pp. 2498–2508, February 2014.

[28] J. W. Leachman, R. T. Jacobsen, S. G. Penoncello, and E. W. Lemmon, "Fundamental equations of state for parahydrogen, normal hydrogen, and orthohydrogen," *Journal of Physical and Chemical Reference Data*, vol. 38, pp. 721–748, September 2009.

[29] U. Setzmann and W. Wagner, "A new equation of state and tables of thermodynamic properties for methane covering the range from the melting line to 625 K at pressures up to 100 MPa," *Journal of Physical and Chemical Reference Data*, vol. 20, no. 6, pp. 1061–1155, 1991.

[30] E. W. Lemmon, M. O. McLinden, and W. Wagner, "Thermodynamic properties of propane. III. A reference equation of state for temperatures from the melting line to 650 K and pressures up to 1000 MPa," *Journal of Chemical & Engineering Data*, vol. 54, no. 12, pp. 3141–3180, 2009.

[31] I. W. Ekoto, A. J. Ruggles, L. W. Creitz, and J. X. Li, "Updated jet flame radiation modeling with buoyancy corrections," *International Journal of Hydrogen Energy*, vol. 39, pp. 20570–20577, December 2014.

[32] National Institute of Standards and Technology, "NIST Chemistry WebBook, SRD 69."

[33] F. P. Lees, *Lees' Loss Prevention in the Process Industries*. Elsevier Science & Technology, 3 ed., 2005.

[34] M. J. Hurley, D. T. Gottuk, J. R. H. Jr., K. Harada, E. D. Kuligowski, M. Puchovsky, J. L. Torero, J. M. W. Jr., and C. J. Wieczorek, eds., *SFPE Handbook of Fire Protection Engineering*. Springer, New York, NY, 5 ed., 2016.

[35] J. Travis, D. Piccioni Koch, and W. Breitung, "A homogeneous non-equilibrium two-phase critical flow model," *International Journal of Hydrogen Energy*, vol. 37, no. 22, pp. 17373–17379, 2012.

[36] T. Spicer and D. Miller, "Quantifying the mass discharge rate of flashing two phase releases through simple holes to the atmosphere," *Process Safety Progress*, vol. 37, no. 3, pp. 382–396, 2018.

[37] A. G. Venetsanos, "Homogeneous non-equilibrium two-phase choked flow modeling," *International Journal of Hydrogen Energy*, vol. 43, no. 50, pp. 22715–22726, 2018.

[38] K. B. Yüceil and M. V. Ötügen, "Scaling parameters for underexpanded supersonic jets," *Physics of Fluids*, vol. 14, pp. 4206–4215, October 2002.

[39] A. D. Birch, D. J. Hughes, and F. Swaffield, "Velocity decay of high pressure jets," *Combustion Science and Technology*, vol. 52, no. 1-3, pp. 161–171, 1987.

[40] A. D. Birch, D. R. Brown, M. G. Dodson, and F. Swaffield, "The structure and concentration decay of high pressure jets of natural gas," *Combustion Science and Technology*, vol. 36, no. 5-6, pp. 249–261, 1984.

[41] B. C. R. Ewan and K. Moodie, "Structure and velocity measurements in underexpanded jets," *Combustion Science and Technology*, vol. 45, no. 5-6, pp. 275–288, 1986.

[42] V. Molkov, D. Makarov, and M. Bragin, "Physics and modelling of under-expanded jets and hydrogen dispersion in atmosphere," in *Proceedings of the 24th International Conference on Interaction of Intense Energy Fluxes with Matter*, March 1-6 2009.

[43] W. Houf and W. Winters, "Simulation of high-pressure liquid hydrogen releases," *International Journal of Hydrogen Energy*, vol. 38, pp. 8092–8099, June 2013.

[44] W. Houf and R. Schefer, "Analytical and experimental investigation of small-scale unintended releases of hydrogen," *International Journal of Hydrogen Energy*, vol. 33, pp. 1435–1444, February 2008.

[45] W. S. Winters, "Modeling leaks from liquid hydrogen storage systems," Tech. Rep. SAND2009-0035, Sandia National Laboratories, January 2009.

[46] G. Abraham, "Horizontal jets in stagnant fluid of other density," *Journal of the Hydraulics Division*, vol. 91, no. 4, pp. 139–154, 1965.

[47] M. Hosseini, I. Dincer, G. Naterer, and M. Rosen, "Thermodynamic analysis of filling compressed gaseous hydrogen storage tanks," *International Journal of Hydrogen Energy*, vol. 37, pp. 5063–5071, March 2012.

[48] B. Lowesmith, G. Hankinson, C. Spataru, and M. Stobbart, "Gas build-up in a domestic property following releases of methane/hydrogen mixtures," *International Journal of Hydrogen Energy*, vol. 34, pp. 5932–5939, July 2009.

[49] W. Houf and R. Schefer, "Predicting radiative heat fluxes and flammability envelopes from unintended releases of hydrogen," *International Journal of Hydrogen Energy*, vol. 32, pp. 136–151, January 2007.

[50] S. R. Turns and F. H. Myhr, "Oxides of nitrogen emissions from turbulent jet flames: Part i—fuel effects and flame radiation," *Combustion and Flame*, vol. 87, no. 3, pp. 319–335, 1991.

[51] R. Schefer, W. Houf, B. Bourne, and J. Colton, "Spatial and radiative properties of an open-flame hydrogen plume," *International journal of hydrogen energy*, vol. 31, no. 10, pp. 1332–1340, 2006.

[52] P. P. Panda and E. S. Hecht, "Ignition and flame characteristics of cryogenic hydrogen releases," *International Journal of Hydrogen Energy*, vol. 42, pp. 775–785, January 2017.

[53] A. Molina, R. W. Schefer, and W. G. Houf, "Radiative fraction and optical thickness in large-scale hydrogen-jet fires," *Proceedings of the Combustion Institute*, vol. 31, pp. 2565–2572, January 2007.

[54] F. D. Wayne, "An economical formula for calculating atmospheric infrared transmissivities," *Journal of Loss Prevention in the Process Industries*, vol. 4, pp. 86 – 92, January 1991.

[55] G. Hankinson and B. J. Lowesmith, "A consideration of methods of determining the radiative characteristics of jet fires," *Combustion and Flame*, vol. 159, pp. 1165–1177, March 2012.

[56] C. Bauwens and S. Dorofeev, "CFD modeling and consequence analysis of an accidental hydrogen release in a large scale facility," *International Journal of Hydrogen Energy*, vol. 39, pp. 20447–20454, December 2014.

[57] S. Jallais, E. Vyazmina, D. Miller, and J. K. Thomas, "Hydrogen jet vapor cloud explosion: A model for predicting blast size and application to risk assessment," *Process Safety Progress*, vol. 37, no. 3, pp. 397–410, 2018.

[58] Center for Chemical Process Safety, *Guidelines for Vapor Cloud Explosion, Pressure Vessel Burst, BLEVE, and Flash Fire Hazards*. John Wiley & Sons Ltd., 2010.

[59] C. R. L. Bauwens and S. B. Dorofeev, "Modeling detonation limits for arbitrary non-uniform concentration distributions in fuel–air mixtures," *Combustion and Flame*, vol. 221, pp. 338–345, 2020.

[60] C. R. L. Bauwens and S. B. Dorofeev, "Quantifying the potential consequences of a detonation in a hydrogen jet release," in *Proceedings of the International Conference on Hydrogen Safety (ICHS 2019)*, (Adelaide (Austrailia)), pp. 612–623, September 24 - 26 2019.

[61] Califiornia Insitute of Technology and J. E. Shepherd, "Detonation Database."

[62] N. Iqbal and M. H. Salley, "Fire Dynamics Tools (FDTs): Quantitative Fire Hazard Analysis Methods for the U.S. Nuclear Regulatory Commission Fire Protection Inspection Program," Tech. Rep. NUREG-1805, U.S. Nuclear Regulatory Commission, Washington, DC, December 2004.

[63] T. E. Oliphant, *A guide to NumPy*, vol. 1. Trelgol Publishing USA, 2006.

[64] S. Van Der Walt, S. C. Colbert, and G. Varoquaux, "The NumPy array: a structure for efficient numerical computation," *Computing in Science & Engineering*, vol. 13, no. 2, p. 22, 2011.

[65] P. Virtanen, R. Gommers, T. E. Oliphant, M. Haberland, T. Reddy, D. Cournapeau, E. Burovski, P. Peterson, W. Weckesser, J. Bright, S. J. van der Walt, M. Brett, J. Wilson, K. Jarrod Millman, N. Mayorov, A. R. J. Nelson, E. Jones, R. Kern, E. Larson, C. Carey, İ. Polat, Y. Feng, E. W. Moore, J. VanderPlas, D. Laxalde, J. Perktold, R. Cimrman, I. Henriksen, E. A. Quintero, C. R. Harris, A. M. Archibald, A. H. Ribeiro, F. Pedregosa, P. van Mulbregt, and SciPy 1.0 Contributors, "SciPy 1.0: Fundamental Algorithms for Scientific Computing in Python," *Nature Methods*, vol. 17, pp. 261–272, 2020.

[66] J. D. Hunter, "Matplotlib: A 2D graphics environment," *Computing in Science & Engineering*, vol. 9, no. 3, pp. 90–95, 2007.

[67] "Math.net numerics."

DISTRIBUTION

Email—Internal

Name	Org.	Sandia Email Address
Ethan Hecht	8367	ehecht@sandia.gov
Kristin Hertz	8367	klhertz@sandia.gov
Myra Blaylock	8751	mlblayl@sandia.gov
Brian Ehrhart	8854	bdehrha@sandia.gov
Chris LaFleur	8854	aclafle@sandia.gov
Ben Schroeder	8854	bbschro@sandia.gov
Technical Library	1911	sanddocs@sandia.gov

Email—External

Name	Company Email Address	Company Name
Laura Hill	laura.hill@ee.doe.gov	DOE EERE HFTO
Michael Laughlin	michael.laughlin@ee.doe.gov	DOE EERE VTO
Mark Smith	mark.smith@ee.doe.gov	DOE EERE VTO

Sandia National Laboratories

Sandia National Laboratories is a multimission laboratory managed and operated by National Technology & Engineering Solutions of Sandia LLC, a wholly owned subsidiary of Honeywell International Inc., for the U.S. Department of Energy's National Nuclear Security Administration under contract DE-NA0003525.